LED Airport Lighting Behavior in Real-World Conditions

Carl Snyder, Christopher Scarpone, Robert Samiljan, Stephen Mackey

March 2021

DOT-VNTSC-FAA-21-04

Prepared for:
U.S. Department of Transportation
Federal Aviation Administration
800 Independence Avenue, SW
Washington, DC 20591

50 YEARS 1970 – 2020

U.S. Department of Transportation
Volpe Center

Notice

REPORT DOCUMENTATION PAGE

Form Approved
OMB No. 0704-0188

1. AGENCY USE ONLY (Leave blank)	2. REPORT DATE	3. REPORT TYPE AND DATES COVERED
	March 2021	Final Report

4. TITLE AND SUBTITLE
LED Airport Lighting Behavior in Real-World Conditions

5a. FUNDING NUMBERS
51FB21A420 TK525/UK525
51FB21Z220 TK527/UK527

6. AUTHOR(S)
Carl Snyder, Christopher Scarpone, Robert Samiljan, Stephen Mackey

5b. CONTRACT NUMBER

7. PERFORMING ORGANIZATION NAME(S) AND ADDRESS(ES)
U.S. Department of Transportation
John A Volpe National Transportation Systems Center
55 Broadway
Cambridge, MA 02142-1093

8. PERFORMING ORGANIZATION REPORT NUMBER
DOT-VNTSC-FAA-21-04

9. SPONSORING/MONITORING AGENCY NAME(S) AND ADDRESS(ES)
U.S. Department of Transportation
Federal Aviation Administration
800 Independence Avenue, SW
Washington, DC 20591

10. SPONSORING/MONITORING AGENCY REPORT NUMBER

11. SUPPLEMENTARY NOTES

12a. DISTRIBUTION/AVAILABILITY STATEMENT
This report is made available to the public online at the National Transportation Library's Repository and Open Science Access Portal (ROSA-P) at https://rosap.ntl.bts.gov.

12b. DISTRIBUTION CODE

13. ABSTRACT (Maximum 200 words)
The Federal Aviation Administration sponsored a test of LED variants of certain types of airport lighting (High Intensity Runway Lighting and Medium Intensity Approach Lighting System lamps) to examine their brightness compared to the conventional incandescent lamps they are intended to replace. The test campaign spanned nine calendar months and captured all major cause of reduced visibility – fog, rain, and snow. The testing used a combination of visual-spectrum camera data and visibility measurements from PC-RVRs to compare the appearance of the lamps across a range of weather and visibility conditions. The testing demonstrated that the LED lamps are brighter than the nominally equivalent incandescent lamps they are intended to replace, particularly under severely reduced visibility. The success of the analysis methodology indicates that in the future it may be possible to use an inexpensive camera viewing existing airport lighting to provide a visibility measurement at airports for which a cost-benefit analysis does not recommend a full PC-RVR installation.

14. SUBJECT TERMS
LED, LED Lighting, Airport Lighting, High Intensity Runway Lights, HIRL, Medium-intensity Approach Lighting System, MALS, Runway Visual Range, Visibility

15. NUMBER OF PAGES
62

16. PRICE CODE

17. SECURITY CLASSIFICATION OF REPORT	18. SECURITY CLASSIFICATION OF THIS PAGE	19. SECURITY CLASSIFICATION OF ABSTRACT	20. LIMITATION OF ABSTRACT
Unclassified	Unclassified	Unclassified	Unlimited

SI* (MODERN METRIC) CONVERSION FACTORS

APPROXIMATE CONVERSIONS TO SI UNITS

Symbol	When You Know	Multiply By	To Find	Symbol
		LENGTH		
in	inches	25.4	millimeters	mm
ft	feet	0.305	meters	m
yd	yards	0.914	meters	m
mi	miles	1.61	kilometers	km
		AREA		
in²	square inches	645.2	square millimeters	mm^2
ft²	square feet	0.093	square meters	m^2
yd²	square yard	0.836	square meters	m^2
ac	acres	0.405	hectares	ha
mi²	square miles	2.59	square kilometers	km^2
		VOLUME		
fl oz	fluid ounces	29.57	milliliters	mL
gal	gallons	3.785	liters	L
ft³	cubic feet	0.028	cubic meters	m^3
yd³	cubic yards	0.765	cubic meters	m^3
		NOTE: volumes greater than 1000 L shall be shown in m^3		
		MASS		
oz	ounces	28.35	grams	g
lb	pounds	0.454	kilograms	kg
T	short tons (2000 lb)	0.907	megagrams (or "metric ton")	Mg (or "t")
oz	ounces	28.35	grams	g
		TEMPERATURE (exact degrees)		
°F	Fahrenheit	5 (F-32)/9 or (F-32)/1.8	Celsius	°C
		ILLUMINATION		
fc	foot-candles	10.76	lux	lx
fl	foot-Lamberts	3.426	candela/m^2	cd/m^2
		FORCE and PRESSURE or STRESS		
lbf	poundforce	4.45	newtons	N
lbf/in²	poundforce per square inch	6.89	kilopascals	kPa

APPROXIMATE CONVERSIONS FROM SI UNITS

Symbol	When You Know	Multiply By	To Find	Symbol
		LENGTH		
mm	millimeters	0.039	inches	in
m	meters	3.28	feet	ft
m	meters	1.09	yards	yd
km	kilometers	0.621	miles	mi
		AREA		
mm^2	square millimeters	0.0016	square inches	in^2
m^2	square meters	10.764	square feet	ft^2
m^2	square meters	1.195	square yards	yd^2
ha	hectares	2.47	acres	ac
km^2	square kilometers	0.386	square miles	mi^2
		VOLUME		
mL	milliliters	0.034	fluid ounces	fl oz
L	liters	0.264	gallons	gal
m^3	cubic meters	35.314	cubic feet	ft^3
m^3	cubic meters	1.307	cubic yards	yd^3
mL	milliliters	0.034	fluid ounces	fl oz
		MASS		
g	grams	0.035	ounces	oz
kg	kilograms	2.202	pounds	lb
Mg (or "t")	megagrams (or "metric ton")	1.103	short tons (2000 lb)	T
g	grams	0.035	ounces	oz
		TEMPERATURE (exact degrees)		
°C	Celsius	1.8C+32	Fahrenheit	°F
		ILLUMINATION		
lx	lux	0.0929	foot-candles	fc
cd/m^2	candela/m^2	0.2919	foot-Lamberts	fl
		FORCE and PRESSURE or STRESS		
N	newtons	0.225	poundforce	lbf
kPa	Kilopascals	0.145	poundforce per square inch	lbf/in^2

*SI is the symbol for the International System of Units. Appropriate rounding should be made to comply with Section 4 of ASTM E380. (Revised March 2003)

Acknowledgments

The authors would like to thank Leo Jacobs of Science Applications International Corporation (SAIC) for his invaluable support of the operations at the Aviation Weather Research Facility over many years, including this effort.

The authors would also like to thank the FAA sponsors and their supporting teams, including Ryan King, Jim Newman, Scott Smith, and Nick Subbotin; Donald Lampkins, Samuel Foster, Dermot Mitchell, and Thomas Tekach; and Matt Harmon, Christopher McLellan, and Gerard Holtorf for their support in establishing data collection and their valuable feedback.

Contents

List of Figures

List of Tables

List of Abbreviations

Abbreviation	Term
AWRF	Aviation Research Weather Facility
CR	Contrast ratio
HIRL	High Intensity Runway Lights
KFMH	Airport code for Cape Cod Coast Guard Air Station (in Falmouth, Massachusetts)
LED	Light-emitting diode
MALS	Medium-Intensity Approach Lighting System
METAR	METeorological Aerodrome Report
MOR	Meteorological optical range
NBP	New Bedford Panoramex
PAT	Patriot Taxiway Industries
PC-RVR	Personal Computer-based Runway Visual Range system
PNT	Positioning, navigation, and timing
JBCC	Joint Base Cape Cod
RMS	Root-mean-square
RVR	Runway Visual Range

1. Executive Summary

This report details an LED lighting test effort at the Volpe Aviation Weather Research Facility (AWRF). A nine-month period of visible-spectrum camera video data and associated visibility data enabled an analysis to compare LED lighting to nominally equivalent incandescent lighting under a wide variety of real-world conditions. All lamps were tested at maximum intensity settings to assess the relative behavior of the lamps under the most challenging visibility conditions.

The video data was associated with visibility to generate curves relating visibility, as measured by the PC-RVR instruments on the test field, to contrast ratio as measured by the visible-spectrum camera. Because contrast is what allows humans to distinguish targets from their backgrounds, the relative positioning of the curves provides a way to compare the inherent brightness of the lamps – a lamp with higher contrast at the same measured PC-RVR visibility will be more visible to a human observer. The use of contrast ratio as a metric was validated by human review of a limited portion of the dataset to verify that contrast ratio tracked well with an observer's judgment of relative brightness.

Although a number of limitations associated with the evolution of the data collection over time mean no strong absolute conclusions can be drawn, the analysis demonstrates that across all weather conditions, LED lamps are brighter than their nominal incandescent equivalents. This agrees with prior laboratory studies and operational demonstrations by the FAA. The success of the relatively inexpensive setup in measuring visibility using only a camera observing runway or approach lighting may indicate a future opportunity for low-cost visibility measurement at airfields where it is infeasible to have PC-RVR instrumentation.

2. Introduction

Airport lighting is critical for surface operations, landings, and departures in reduced-visibility conditions and at night. It is a violation of FAA regulations for airports to be open and for both commercial air services and private pilots to operate out of airports without adequate lighting at night or during periods of reduced visibility[1]. As a result, lighting infrastructure at airports is a significant investment, both in terms of installation and operating costs.

Light-emitting diode (LED) lamps and appropriate fixtures have become increasingly popular in recent times because of their substantially higher luminous efficacy (approximately 85 – 150 lm/W depending on lamp and fixture) and usable lifetime (approximately 25,000 – 60,000 hours) compared to incandescent lighting products, which have a luminous efficacy of 15 – 20 lm/W and usable life from 1,000 – 8,400 hours. (Pattison, et al., 2018). The substantially reduced operating costs resulting from reduced electricity use and maintenance make LED lamps attractive as replacements for existing conventional incandescent or halogen lamps. In addition to the financial benefits motivating the transition, the 2007 Energy Independence and Security Act mandates the phase-out of incandescent lamps of certain wattages, and manufacturers of airport lighting systems are complying with the requirements by transitioning to LED lamps.

LED lamps, however, have different characteristics from incandescent lamps that are potentially relevant to their suitability as replacements for incandescent lamps in aviation use. In particular, the spectral characteristics of LED and incandescent lamps are different, in both the visual and infrared spectra, and their thermal characteristics are different because of their different mechanisms of generating light. The FAA has been researching the suitability of LED lamps as replacements for incandescent lighting since 2004, as airports have been gradually transitioning some incandescent lighting to LED lamps.

Previous laboratory research sponsored by the FAA produced a series of academic research papers, mostly authored by Dr. John D. Bullough at the Lighting Research Center at the Rensselaer Polytechnic Institute in Troy, NY. The FAA also conducted operational demonstrations in Alaska and at the William J. Hughes Technical Center in Atlantic City, NJ. To supplement the data collected in these studies, the FAA sponsored a data-collection effort, employing a visual-spectrum camera, weather sensors, and select LED airport lighting, at the John A. Volpe National Transportation Systems Center's Aviation Weather Research Facility (AWRF), in Sandwich, MA.

This effort was initially framed as a qualitative assessment of the subjective appearance of the LED lamps. Data collection was aimed at covering many different visibility and weather conditions so that a human observer could review the video and evaluate the relative appearance of the LED and incandescent lamps. However, the FAA and

[1] 14 C.F.R. § 121.97 – Airports: Required Data; 14 C.F.R. §139.311 – Marking, signs, and lighting

Volpe decided that the video and matched weather data provided a potential opportunity for automated review of the entirety of the dataset to provide a quantitative, objective assessment of the relative apparent brightness of the lamps.

The effort focuses particularly on video data captured during reduced-visibility conditions, when airport lighting is most important. As the FAA has already evaluated LED lamp performance at lower intensity settings, all lamps were tested at their highest intensity settings used in severely reduced visibility. This report describes the data collection, analysis methodology, and results of the comparison for the two types of lamps tested – lamps from the Medium-Intensity Approach Lighting System (MALS) and High Intensity Runway Lights (HIRLs).

3. Experimental Setup

3.1 The Aviation Weather Research Facility

The Volpe Aviation Weather Research Facility (AWRF) is a 150-acre site located on a relatively flat ridge at Joint Base Cape Cod (JBCC) in Sandwich, Massachusetts. The AWRF is known for inclement weather conditions throughout the year, making it an ideal outdoor laboratory for the evaluation of technology under challenging conditions. The weather research facility consists of an operations building and several measurement sites, each of which contain one or more weather sensors. Data from the various sensors is transmitted to servers in the operations building. Volpe's Aviation Weather & PNT Applications division (V345) manages the AWRF and coordinates collaboration across a variety of the Center's divisions to access subject matter expertise in meteorology, information technology, mechanical and electrical engineering, data management and analysis, construction engineering, airport operations management, aviation operations and flight deck technology, air traffic control and management, systems engineering, and human factors as appropriate.

Figure 3-1: The AWRF and surrounding area within JBCC

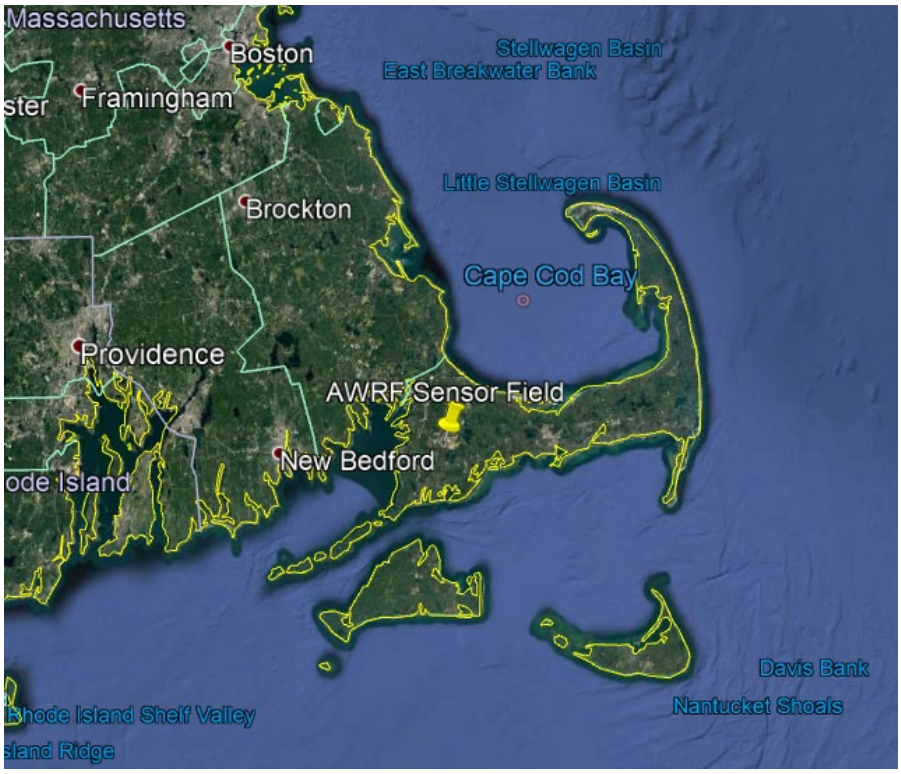

Figure 3-2: The AWRF is located in the western portion of Cape Cod

3.1.1 Climatology

The goal of the data collection effort was to collect visual spectrum video data of the lamps in a wide range of weather conditions. The AWRF is well-suited to data collection during challenging, low-visibility weather. Average precipitation is approximately 4 inches of liquid-equivalent precipitation per month throughout the year (approximately 48 inches total annually), with slightly elevated precipitation in November and December and March and April and slightly reduced precipitation in June and July. Significant snowfall typically occurs December through March, with an annual total of approximately 37 inches.

One particularly attractive aspect of weather at the AWRF for low-visibility testing efforts is the frequency of dense fog and other periods of significantly reduced visibility. Ceiling < 100 feet and visibility < 0.25 mi occurs about 0.3% of the time on an annualized basis (about 26 hours per year), with reduced visibility particularly common September – February and May – June, and less typical in March – April and July – August. Table 3-1 shows the likelihood of this extremely low visibility at various times of day throughout the year.[2]

[2] US Air Force, Operational Climatic Data Summary – II (OCDS-II) for KFMH, period of record 1/1/2010 – 12/31/2019

Table 3-1: Frequency of Very Low Visibility (Ceiling < 100 ft & Visibility < 0.25 miles)

% Frequency Observed During This Time Period													
Occurrence Time	Jan	Feb	Mar	Apr	May	Jun	Jul	Aug	Sep	Oct	Nov	Dec	Ann
17-19 LST[3]	0.2	0	0	0.1	0.4	0.2	0	0	0	0	0	0	0.1
20-22 LST	0.7	0.8	0	0.1	0.5	0.3	0	0	0.9	0.3	0	0.4	0.3
23-01 LST	0.4	0.5	0	0	0.1	0.9	0	0.2	1.1	0.5	0.2	0.7	0.4
02-04 LST	0.4	0.5	0	0.3	1.5	1.4	0.5	0.6	0.7	0.8	0.8	0.4	0.7
05-07 LST	0.6	0.8	0	0.6	0.8	0.6	0.2	0.2	1.5	1.2	1	0.6	0.7
08-10 LST	0.2	0.5	0	0	0	0.1	0.1	0	0.1	0.1	0.1	0.2	0.1
11-13 LST	0.1	0.1	0.1	0.5	0	0	0	0	0	0	0	0.3	0.1
14-16 LST	0.1	0.9	0.1	0	0.1	0	0	0	0	0	0.1	0.1	0.1
All Hours	0.3	0.5	0	0.2	0.4	0.4	0.1	0.1	0.5	0.4	0.3	0.3	0.3

Less-severely reduced visibility is even more common. Table 3-2 shows the likelihood of ceiling < 3,000 ft and visibility < 3 miles. Visibility this low is observed over a quarter of the time.

Table 3-2: Frequency of Low Visibility (Ceiling < 3,000 ft & Visibility < 3 miles)

% Frequency Observed During This Time Period													
Occurrence Time	Jan	Feb	Mar	Apr	May	Jun	Jul	Aug	Sep	Oct	Nov	Dec	Ann
17-19 LST	27.3	23.7	23.7	22.7	29.4	25.7	22	21.6	22.3	26.6	19.2	24.5	24.1
20-22 LST	25.5	25.9	23.2	24.2	39.7	29.5	26.6	23.4	27.5	26.9	19.6	25.5	26.4
23-01 LST	25.3	26.2	26.2	28	43	34.8	29.8	27.8	30.5	29.1	25.1	26.7	29.3
02-04 LST	25.8	26.3	28.4	26.9	44.2	38.3	36	30.8	33.1	30.8	26.1	28	31.2
05-07 LST	24.7	27.2	27.2	25.9	39.3	31.9	29.2	27.4	29.4	28	25.9	27.4	28.6
08-10 LST	22.9	26.6	28.2	24.4	32.5	28.5	24.9	24.8	27.8	28.8	24.9	23.9	26.5
11-13 LST	24.9	23.9	28.6	22.1	26.7	24.1	19.1	18.7	26	24.8	22.4	24.7	23.8
14-16 LST	24	23.6	25	20.5	25.3	22.8	16.8	18.8	23.6	24.9	19.9	24.2	22.5
All Hours	25	25.4	26.3	24.3	35	29.4	25.5	24.2	27.5	27.5	22.9	25.6	26.5

3.1.2 Instrumentation

The AWRF has an extensive suite of weather sensors that are vital to its function as an outdoor laboratory. During the data collection period, the following sensors were active and collecting data:

- A visible-spectrum camera (AIDA UHD-100)
- Three Vaisala FA-19200 PC-RVR visibility sensors (forward scatter meters)

[3] Local Standard Time. UTC – 5.

- A Droplet Measurement Technologies FM-120 fog spectrometer
- A Vaisala WXT520 weather station
- An OTT Parsivel² Disdrometer/Present Weather Sensor

The analysis effort focuses on the recorded video from the visible-spectrum camera and the PC-RVR visibility measurements.

In addition to the instrumentation present at the AWRF, the METAR (METeorological Aerodrome Report) reporting from KFMH, the station at Otis Air National Guard Base about 1.5 miles away, was used to group data into broad categories of adverse weather.

3.2 Test Design and Site Layout

The FAA supplied Volpe with the test lamps and required supporting electrical infrastructure (including a constant current regulator). In order to test the lamps, Volpe designed a "simulated runway". This was an unobstructed, cleared region approximately 200 feet wide and over 2,400 feet long. At one end was the observation point, a 30-foot tower. The visible-spectrum camera and one PC-RVR, as well as data collection equipment, were mounted on the top platform of the tower.

Twelve lamps were tested, arranged in a two-row array. The lamps chosen for testing were designed for use in two different applications. Eight of the lamps were Medium Intensity Approach Lighting System (MALS) lamps, of which six were LED lamps from two different manufacturers – three from Patriot Taxiway Industries (PAT), and three from New Bedford Panoramex (NBP) – and two were commercially available incandescent lamps (150W GE Floodlight 150 PAR38 halogen bulbs with a nominal 10 degree beamwidth). Four were High Intensity Runway Edge Lighting (HIRL) lamps; two LED lamps (one manufactured by Astronics, the other by ADB Safegate) and two incandescent lamps provided by the FAA, at operating power of 150W and 200W.

The closer row, at 1,800 feet from the observation tower, had an array of seven lamps. A cluster of three MALS lamps on the left as viewed from the tower and the four HIRL lamps on the right. The farther row, at 2,400 feet from the tower, was an array of five MALS lamps. Two of the MALS lamps at the edges of the rear row were oriented such that the edge of their beam was pointed at the camera, rather than the center of the beam. This was intended to help explore glare/edge effects of the LEDs.

Because the ability of airport lighting to "cut through" reduced-visibility conditions under significantly impaired visibility is vital to safe, efficient airport operation, all lamps with variable brightness were operated at their highest brightness step for the duration of the testing. Some lamps were replaced during testing because of bulb failures.

Three PC-RVR visibility sensors were the primary instruments used to measure visibility during data collection. One PC-RVR was co-located with the visual spectrum camera on the tower; one was mid-field, approximately 1,000 feet downrange from the tower; and one was located at the edge of the 2400' row of lights.

Figure 3-3 shows the test arrangement, and Figure 3-4 shows a representative view from the visual spectrum camera.

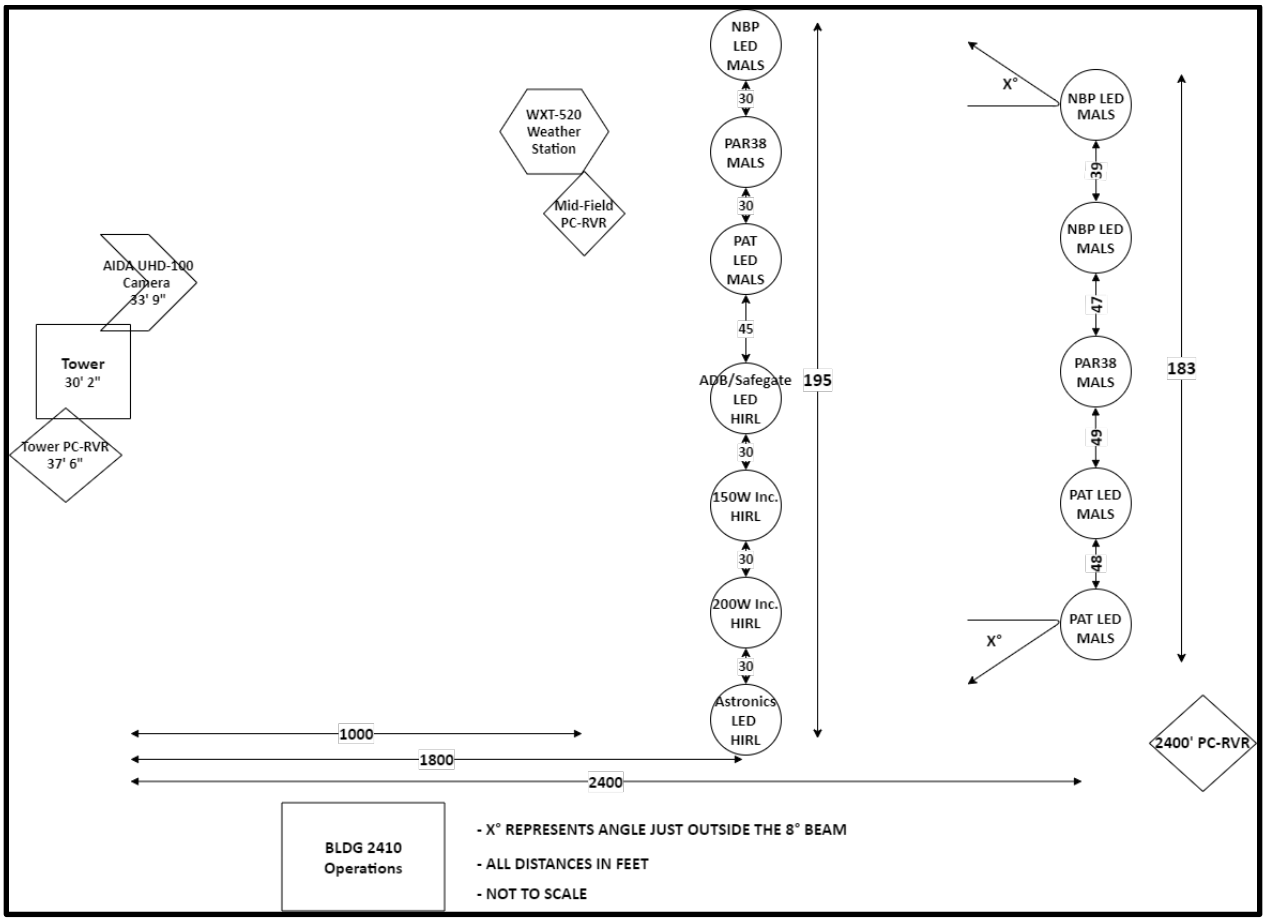

Figure 3-3: Diagram of AWRF Test Layout

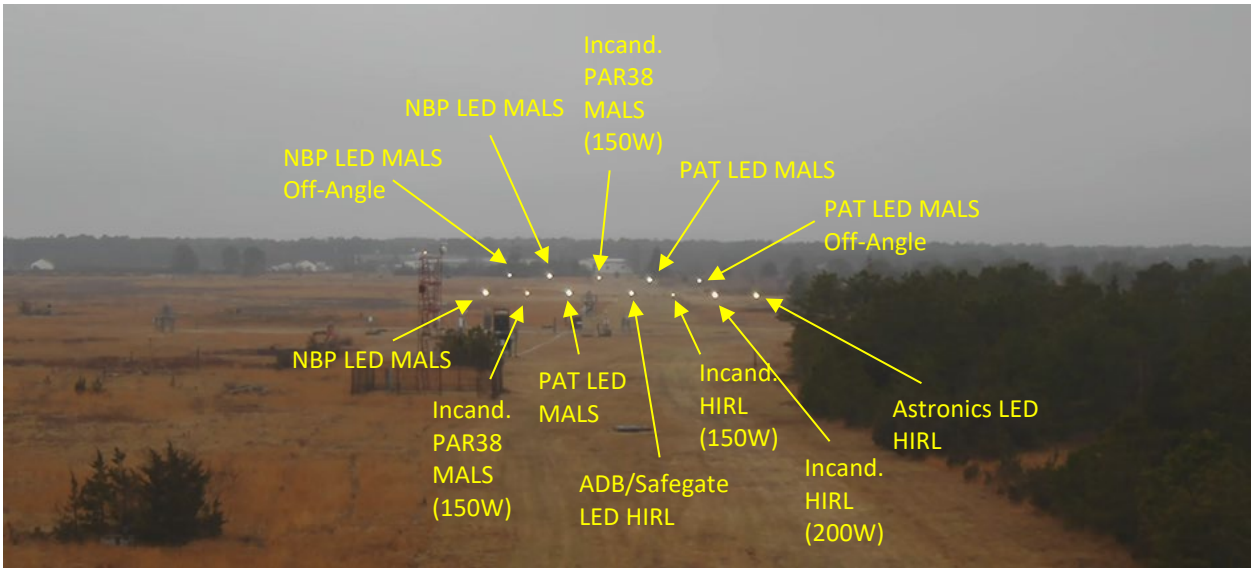

Figure 3-4: Visual Spectrum Camera View

4. Data Collection Overview

Data was continuously collected over the course of approximately 9 months (293 days) between April 2019 and January 2020.

4.1 Low Visibility Event Identification

The data analysis effort was intended to characterize the behavior of LED lamps, compared to incandescent lamps, under adverse weather conditions. The FAA has equipment to measure Runway Visual Range (RVR) at many airports in the United States. RVR informs pilot decisions about which airports they can safely depart from, or arrive to, in adverse weather. FAA reporting of RVR begins when RVR drops below 6,000 feet (or when prevailing visibility is 1 mile or less regardless of the RVR as measured by the instrumentation at the airfield).

Even with automation, loading and processing large amounts of video data is time-consuming. In order to facilitate data processing and analysis, periods of low visibility were identified using the PC-RVR visibility. First, the PC-RVR data were time-matched. The PC-RVRs report visibility every 15 seconds, which is a trailing average of the last minute of measurements, but their reporting schedule is not exactly synchronized between systems, so the closest-in-time visibility reports, with a maximum time difference of 2 minutes, were matched. The mid-field PC-RVR was used as the master dataset. Low-visibility events were defined by screening out all PC-RVR measurements with a reported visibility of greater than 6,000 feet. A rise in visibility to over 6,000 feet for at least five minutes was used to determine the end of an event.

There were 304 distinct low-visibility events identified during the data collection period, with a collective duration of approximately 10 days (240 hours), 3.4% of the total data collection time. Video data was available for 262 of these events, with a collective duration of approximately 8.6 days (207 hours), 2.9% of the total data collection time.

There were 163 fog events, with a total duration of approximately 7.4 days (178 hours), 2.5% of the total data collection time. Video data was available for 148 of these events, with a collective duration of approximately 6.8 days (162 hours), 2.3% of the total data collection time.

There were 104 rain events, with a total duration of approximately 2.2 days (53 hours), 0.8% of the total data collection time. Video data was available for 93 of these events, with a collective duration of approximately 2.0 days (47 hours), 0.7% of the total data collection time.

There were 7 snow events, with a total duration of approximately 0.5 days (13 hours), 0.2% of the total

data collection time. Video data was available for 6 of these events, with a collective duration of approximately 0.4 days (10 hours), 0.1% of the total data collection time. The winter of 2019 – 2020 had unusually light snowfall, and data collection ended in January, before the end of the snow season. In addition, snow does not typically reduce visibility to below 6,000 feet at the AWRF.

Not all periods of reduced visibility were associated with adverse weather. There were 55 events, with a total duration of 1.0 days (24 hours), without any adverse weather reported on the KFMH METAR, representing 0.3% of the total data collection time. Video data was available for 41 of these events, with a collective duration of approximately 0.6 days (14 hours), 0.2% of the total data collection time.

4.2 Weather Identification

As previously noted, METAR data from KFMH was used to categorize weather types for periods of low visibility for the purposes of assessing the relative behavior of the lamps under differing weather conditions. Because of the proximity of KFMH to the AWRF, there is good agreement between METAR reports of precipitation and/or obscuration and the observation of low-visibility events at the AWRF.

A summary table of the precipitation and obscuration types reported in a METAR, taken from the Federal Meteorological Handbook, is presented in Figure 4-1 below.

QUALIFIER		WEATHER PHENOMENA		
INTENSITY OR PROXIMITY 1	DESCRIPTOR 2	PRECIPITATION 3	OBSCURATION 4	OTHER 5
- Light Moderate (see note 2) + Heavy VC In the Vicinity (see note 3)	MI Shallow PR Partial BC Patches DR Low Drifting BL Blowing SH Shower(s) TS Thunderstorm FZ Freezing	DZ Drizzle RA Rain SN Snow SG Snow Grains IC Ice Crystals PL Ice Pellets GR Hail GS Small Hail and/or Snow Pellets UP Unknown Precipitation	BR Mist FG Fog FU Smoke VA Volcanic Ash DU Widespread Dust SA Sand HZ Haze PY Spray	PO Well- Developed Dust/Sand Whirls SQ Squalls FC Funnel Cloud Tornado Waterspout (see note 3) SS Sandstorm SS Duststorm

1. The weather groups shall be constructed by considering columns 1 to 5 in the table above in sequence, i.e. intensity, followed by description, followed by weather phenomena,
   e.g. heavy rain shower(s) is coded as +SHRA
2. To denote moderate intensity no entry or symbol is used.
3. Tornados and waterspouts shall be coded as +FC.

Figure 4-1: METAR Weather Codes

For the purposes of this analysis, precipitation and obscuration codes were divided into three main categories:

- Fog: BR, FG, HZ
- Rain: DZ, RA
- Snow: GS, IC, PL, SG, SN

These categories are not exclusive; for example, a fog with drizzle (DZFG) would be labeled as both a fog and a rain event. Given the relatively low time resolution of METAR reporting (typically one report per hour), any precipitation or obscuration type reported during a particular low-visibility event is assigned as a descriptor of that event.

An example of the correlation between the visibility, as measured by the mid-field PC-RVR, and METARs with reported adverse weather, is shown in Figure 4-2. The solid blue line is the visibility in feet as measured by the PC-RVR plotted for several days in April 2019, close to the beginning of data collection, and the red points are METARs with reported precipitation or obscuration. It is evident that, generally, although adverse weather does not always reduce visibility below 6,000 feet, there typically (though not always) *is* adverse weather on the METAR when visibility is low. Periods of low visibility without reported adverse weather generally occurred at night, making it impossible to conclusively determine the cause in most cases, but considerably inhomogeneous weather was observed even within the bounds of the sensor field. It is likely that the periods of reduced visibility were associated with local weather phenomena not observed at KFMH.

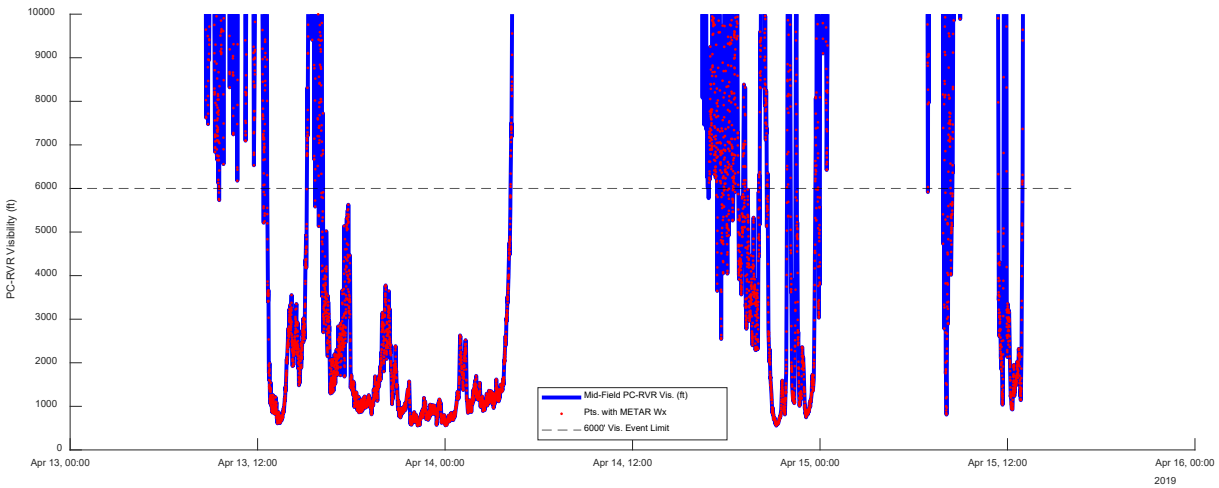

Figure 4-2: Correlation of Low Visibility with Adverse Weather

5. Analysis Methodology

5.1 Overall Philosophy

The data collection effort initially focused on qualitative assessment of the differences between LED and incandescent lamps. Observation of the video collected during the periods of low visibility suggested that the LED lamps appeared brighter, on average, than their nominally equivalent incandescent counterparts. This is consistent with previous research on the subject, which found in laboratory experiments that, generally speaking, LED lamps are perceived as brighter than incandescent lamps at the same luminous intensity (Matching LED and Incandescent Aviation Signal Brightness, 2014).

Extension of these subjective results, obtained by viewing a relatively small subset of the collected video data, required development of an analysis methodology to answer, in an objective way, these questions:

1) Does the perceived brightness of LED lamps differ from their incandescent equivalents?
2) If the two kinds of lamps differ, how so?
    a. Are the LED lamps brighter or dimmer on average than their incandescent equivalents?
    b. Do the differences between LED and incandescent lamps (if any) differ based on prevailing visibility or weather conditions?

Because the data collection effort was not originally designed for a quantitative assessment, it has some features that are not ideal for an attempt to measure the absolute performance of the lamps. For example, camera settings (aperture, exposure time, shutter speed, white balance, etc.) were variable throughout the data collection as we optimized the camera image for changing ambient lighting and weather conditions. Camera settings were particularly variable through the earliest part (approximately 1 month) of data collection before we fine-tuned settings. Records of all the changes made are not easily accessible (though they are embedded in the video files, the change times are not known, making it infeasible to generate a list of the camera parameters over time).

As a result of these data set challenges, the analysis focuses on a *relative* assessment, without assigning particular significance to the absolute values of the observed lamp brightness. This analysis is possible because all of the frames analyzed were collected at the same time, with the same camera settings for all of the lamps. Any camera settings changes affect all of the lamps for a particular frame. In addition, the large size of the dataset and the relative stability of camera settings for the majority of data collection allow us to have confidence in the relative behavior of the lamps at the median level. Analysis techniques are used to exclude outliers associated with camera misbehavior, bad camera settings, or unusual occurrences (e.g. the obscuration of an individual lamp relative to others by raindrops or snow

in the near field or animal movement across the field of view).

5.2 Key Metric: RMS Contrast Ratio

Since differences in contrast are what allow human beings to distinguish objects from their backgrounds, root-mean-square (RMS) contrast ratio was chosen as the metric to address the questions posed by this analysis. Contrast can be by differences in luminance, differences in color, or both. Humans are substantially more sensitive to differences in luminance than differences in color. Additionally, in the most challenging low-visibility conditions, the background of the lamp is obscured by the fog or other cause of reduced visibility, largely eliminating color contrast. The analysis therefore uses luminance-based contrast.

Many different definitions of contrast ratio have been proposed and used; for example,
Weber contrast (used in comparing a well-defined target to a background):

$$\frac{(L_{object} - L_{background})}{L_{background}} \quad (1)$$

where L denotes the luminance of the target region;

Michelson contrast (used for gratings and other periodic stimuli):

$$\frac{L_{max} - L_{min}}{L_{max} + L_{min}} \quad (2)$$

where L_{max} and L_{min} are the highest and lowest luminance in the image, respectively;

and RMS contrast:

$$\sqrt{\frac{1}{N}\sum_{i=1}^{N}\frac{(L_i - \bar{L})^2}{\bar{L}^2}} \quad (3)$$

where for a region of N pixels, L_i is the luminance of the pixel and $\bar{L}$ is the average luminance of the entire region.

This analysis uses RMS contrast. Initial exploration showed that RMS contrast ratio values tracked more closely with PC-RVR visibility and were subjectively more consistent with relative lamp brightness than Weber contrast. In addition, RMS contrast "predicts human contrast detection thresholds…better than other common measures of contrast" (Local luminance and contrast in natural images, 2006).

One advantage of RMS contrast ratio is that it does not require a definition of the target and the

background. This is important for our application, because the apparent size of the lamps varies with lighting conditions and visibility. Their apparent diameter varies from 0 (in very low visibility) to roughly 8 pixels. However, it would be inappropriate to calculate the RMS contrast ratio of the entire scene to characterize the relative brightness of individual lamps. In order to capture the lamps and their immediate surroundings, to make the metric accurately reflect the visibility of each lamp, a 30 x 30 pixel box was drawn around the center of each lamp, and the RMS contrast ratio was calculated only for this box.

5.3 Human Perception Weighting

The video was gamma-compressed on encoding according to Recommendation ITU-R BT.709-6. In order to compute contrast ratios based on luminance, the RGB video data must be converted to greyscale. In order to compute contrast ratio based on luminance (rather than luma), the gamma compression must be removed from the video data. The de-compression was performed using the reference transfer function in Recommendation ITU-R BT.1886 with unity gain and zero black level lift (i.e. a simple γ = 2.4), since the de-compression is done for mathematical analysis rather than display.

After the RGB values were re-linearized, they were used to compute a luminance using the BT.709-6 recommendation values:

$$L = 0.2126R + 0.7152G + 0.0722B \quad (4)$$

This weighting accounts for the much higher sensitivity of the human eye to green light compared to red and blue light. RMS contrast ratios for the individual lamps were then computed using the 8-bit greyscale luminance values.

5.4 Validation of RMS Contrast Ratio as a Metric

In order to validate RMS contrast ratio as an appropriate metric to characterize the relative brightness of lamps, sample video frames were consulted to verify that RMS contrast ratio correctly reflected the relative apparent brightness of the lamps as perceived by a person watching the video. An example screenshot cropped to the region around the lamps is shown below.

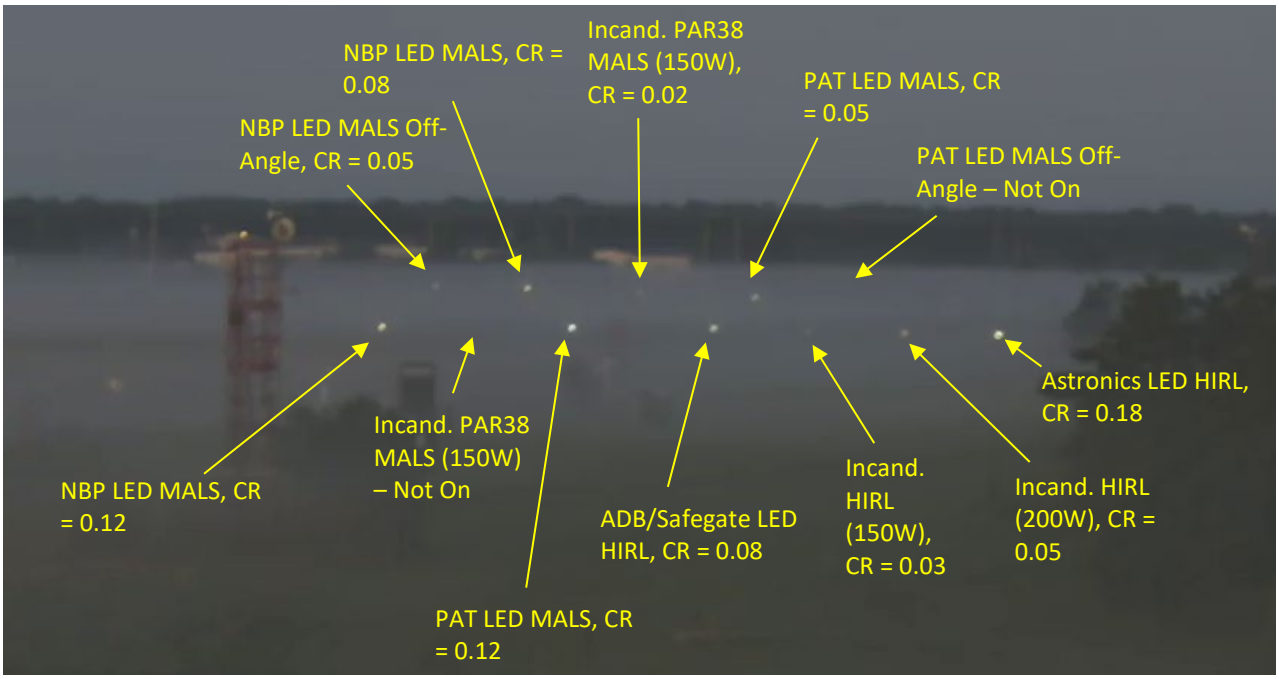

Figure 5-1: Example Screenshot with RMS Contrast Ratio Values

All of the illuminated lamps are visible, though some are very faint. The values of the RMS contrast ratio accurately reflect the relative brightness of the individual lamps, and a threshold of 0.02 is roughly the level where the lights are just barely distinguishable from their surroundings, which agrees with previously-published literature (Measuring Contrast Sensitivity, 2013).

5.5 Relationship Between Contrast Ratio and Visibility

In aviation meteorology, the century-old Koschmieder model is widely accepted to relate visibility (as measured by a trained observer) to a measurable atmospheric parameter. "Visibility" is generally defined as the distance at which a target is barely distinguishable from its background. If we assume that the atmosphere is homogeneous, and a constant proportion of the light emitted by a target, but not the background, (or the background, but not the target) is attenuated per unit distance, both the luminance of the target (or background) and the contrast are reduced as a simple inverse exponent:

$$C_a = C_i e^{-\sigma X} \tag{5}$$

Here, C_a is the apparent contrast; C_i is the inherent contrast (the difference in luminance between the object and background, normalized by background luminance, without atmospheric attenuation), σ is called the "extinction coefficient" and has units of inverse distance, and X is the distance to the target.

Koschmieder originally considered a perfectly black target against a bright sky, and defined $C_i = -1$. It is important in the derivation of Koschmieder's law that either the luminance of the target or the luminance of the background is not attenuated with distance. For Koschmieder's original setting (dark object against the sky), this was a reasonable assumption – the luminance of the sky from the atmospheric scattering is approximately constant. For our case, the background is not the sky, but the ground. However, the background is relatively dark compared to the lamps, meaning that under certain conditions (dark night, severely reduced visibility), the background luminance will be approximately constant at near-zero and only the lamp luminance will be attenuated. The simple Koschmieder model will be less accurate if our background is bright (e.g. as the result of snow on the ground); however, it still provides us with a starting point for expected behavior.

If we then set the apparent contrast C_a to the barely-distinguishable contrast threshold C_t and rearrange for the distance X at which that contrast is apparent, we get the conventional equation for meteorological optical range (MOR):

$$MOR = \frac{1}{\sigma}\ln\left(\frac{C_i}{C_t}\right) \tag{6}$$

or equivalently

$$MOR = \frac{-1}{\sigma}\ln\left(\frac{C_t}{C_i}\right) \tag{7}$$

Classical sources use different values for C_t, with typical values of either 0.02 or 0.05; these reduce to approximately

$$MOR = \frac{3.91}{\sigma}\ (8) \text{ and } MOR = \frac{3.00}{\sigma}\ (9)$$

respectively. The PC-RVR sensors used by the FAA convert from extinction coefficient to "visibility" (MOR) using Equation 9.

For measuring differences between the lamps, rather than measuring extinction coefficient and calculating MOR, we are measuring apparent contrast, C_a, directly. In this case, C_i, the inherent contrast of the lamp, is the parameter we are trying to estimate. Since the lamps are effectively co-located (at least in each row), we assume the atmosphere is homogeneous within a row and therefore σ = constant. If we combine the apparent contrast equation and Koschmieder's Law, we have

$$C_a = C_i e^{-\frac{3.00}{MOR}X} \tag{10}$$

X is a constant for all lights in the same row, so we have the relationship

$$C_a \propto C_i e^{-\frac{1}{MOR}} \tag{11}$$

We observe that a larger value of C_a at the same independently-measured MOR implies a larger C_i – in other words, a more visible lamp. The parameter $e^{-\frac{3.00}{MOR}X}$ is the *remaining contrast* – the fraction of the inherent contrast that would remain visible to an observer at a distance of X units away at a particular MOR in the same units.

While the contrast ratios in Koschmieder's law are Weber contrast ratios rather than RMS contrast, drawing a small sample box around the known positions of the lamps effectively simulates Weber contrast by restricting the domain of the RMS computation to each lamp and its immediate background, while retaining the advantage that a precise target region does not need to be specified. We expect to see the same kind of relationship between RMS contrast ratio and MOR as predicted by Koschmieder's Law, subject to the caveats about background visibility discussed earlier.

A schematic view of the expected relationship is shown in Figure 5-2.

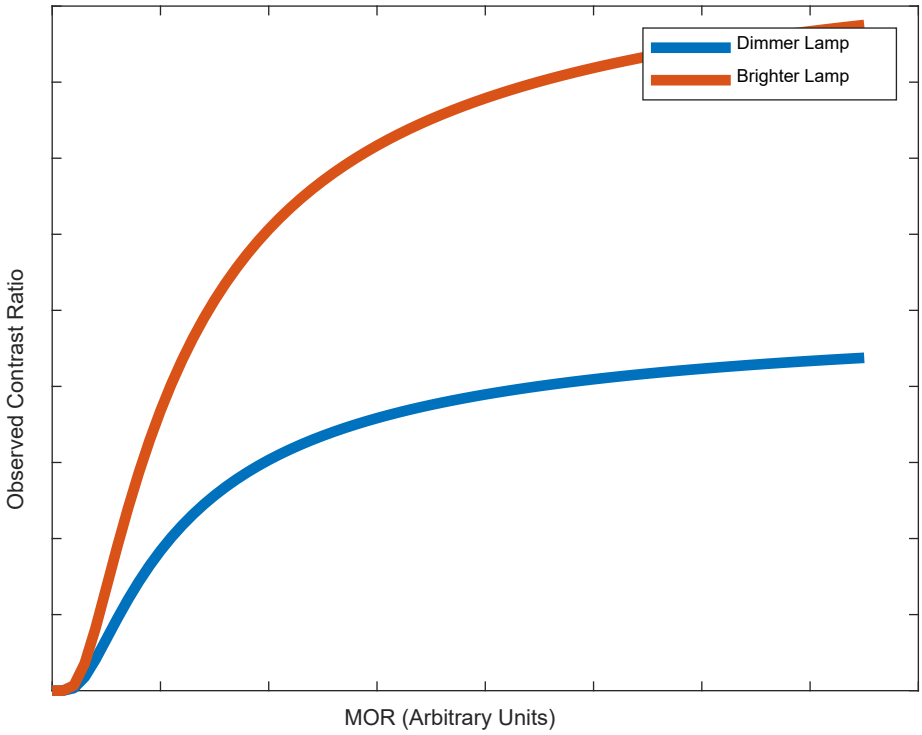

Figure 5-2: Theoretical Relationship between Observed Contrast and MOR

5.6 Time Correlation with Other Sensors

5.6.1 PC-RVR Visibility Data

The PC-RVR instrumentation was periodically unavailable for a variety of reasons (e.g. maintenance, data link outages). In addition, the time reporting of the instruments was slightly asynchronous. The mid-field PC-RVR was used as the master visibility dataset, as its availability was generally a superset of the availability of the tower and 2400' PC-RVRs. For every mid-field PC-RVR measurement, the measurement closest in time, with a maximum time difference of 2 minutes, was taken from the other two PC-RVRs. These three measurements were then used to establish a master table of PC-RVR measurements, with a timestamp that was the average of the PC-RVR measurements present and a visibility value (or empty value) for each PC-RVR.

5.6.2 Weather Data

As previously mentioned, in addition to an all-weather comparison covering the entire dataset, the relative characteristics of the lamps in fog, rain, and snow were also explored. METAR data from KFMH was correlated to each frame of video by taking the closest in time METAR report. If there was missing METAR data and therefore no METAR data matching the sample time to within 31 minutes, the data was kept, but flagged as missing weather information.

5.7 Procedure

The work-flow used to evaluate the relative brightness of the lamps is shown below.

5.7.1 Low-Visibility Event Identification and Weather Correlation

1) Parse the PC-RVR data for the tower, mid-field, and 2400' PC-RVRs
2) Remove all PC-RVR measurements with a visibility over the 6,000' low-visibility threshold
3) Take every mid-field PC-RVR measurement, and find the closest-in-time measurement from the tower and 2400' PC-RVRs, requiring a match to within 2 minutes of the timestamp on the PC-RVR measurement
4) Establish a master table of PC-RVR measurements from all sensors, by using the time-correlated measurements from step 1 and assigning a timestamp by averaging the timestamps of the PC-RVR measurements present
5) Sort the master table in chronological order
6) Separate the master table into discrete low-visibility events by looking for gaps in the time

between measurements of more than five minutes
    a. Eliminate any low-visibility events shorter than five minutes
7) For every point in each event, search the METAR data for the closest matching report within 31 minutes and extract the weather codes and timestamp, flagging any points without associated METAR data

5.7.2 Video Processing and Event Correlation

1) Use the video metadata (timestamping and duration) to establish a master list of available video files including filename, duration, and beginning and end time
2) For each low-visibility event:
    a. Load the appropriate video file, starting from the beginning of the event
    b. In order to increase processing speed, extract one frame from the video data every 15 seconds, iterating through video files as necessary, until the next sample time would be beyond the end of the event, retaining the timestamp of the frame
    c. Extract the 30 x 30 pixel sample boxes around each lamp and save them
    d. Convert the 24-bit RGB images to greyscale and save the greyscale images
        i. Gamma decompression
        ii. Apply BT.709-6 weighting
    e. Compute RMS contrast ratio for each lamp sample box for every frame of video collected
    f. Remove data, on a per-lamp basis, for times when the video is known to be bad for that lamp (e.g. because the lamp was turned off for maintenance, or had burned out, or had suffered a power failure)
    g. For each frame, find the closest-matching PC-RVR measurements, requiring a match within 30 seconds, and create a table for every low-visibility event containing:
        i. The RMS contrast ratio for every valid lamp measurement from a given frame within the event, with matching visibility measurements from the PC-RVR data, and the frame timestamp

5.7.3 Analysis

1) Concatenate all the PC-RVR-correlated RMS contrast ratio tables from each individual event, in order to represent the entire dataset
2) Bin the data into the RVR reporting intervals, from 1,800 feet (slightly lower than the 1800 foot distance from the observation tower to the first row of lamps) and through 6,000 feet. Relevant RVR reporting intervals:
    a. From 800 feet to 3,000 feet; 200-foot intervals
    b. From 3,000 feet to 6,000 feet: 500-foot intervals

Select only those points with visibility from the relevant sensor (both the mid-field and 2400' PC-RVR were used as selection visibilities) that fall into the appropriate bin. Only retain points where the measured visibility is no lower than the bottom of the first relevant bin (i.e. visibility >= 1700' for the 1800' row of lamps and visibility >= 2,300' for the 2400' row of lamps).

Note: RVR reports are rounded to the nearest value; for example, 1,501 feet to 1,699 feet are reported as 1,600 feet. Rounding intervals are asymmetric at the breakpoints; 3,000 feet corresponds to a range of 2,901 feet to 3,249 feet.

3) Filter the data:
    a. Exclude the data collected during the time period of the most significant number and size of camera settings changes (data collected prior to May 24, 2019)
    b. Require at least 400 points in a bin to proceed
        i. Note: for data for specific weather types, this criterion is relaxed to 250 points; however, the relative error is correspondingly larger.
4) Compute a median RMS contrast ratio for the measurements in each bin
5) Plot the median RMS contrast ratio measurement against the centers of the visibility bins

5.7.4 Filtering Rationale

The rationale for the filters applied in the analysis process is provided below.

Filter a) (exclude early data)

- While camera settings continued to change slightly over the course of the data collection period, the first six weeks or so of data collection saw major changes that significantly affected the brightness (and apparent diameter) of the lamps. These points are not useful to characterize the typical lamp behavior.

Filter b) (require at least 400 points in a bin to calculate a median)

- We are attempting to estimate the median value of the RMS contrast ratio for a particular visibility bin for each lamp to compare the apparent contrast across lamps. The sample size required by the Central Limit theorem for a confidence interval W units wide around the true mean for a desired level of confidence characterized by a Z-score, Z is $n = \frac{4Z^2\sigma^2}{W^2}$. The observed data range from RMS CR of 0 to about 1.5, and the observed bin standard deviation σ is approximately 0.5. For a 95% confidence interval with a width of 0.1, Z = 1.96; with σ = 0.5, we

have $n = \frac{4(1.96)^2(0.5)^2}{(0.1)^2}$ = 386, which we round to 400.

6. Results and Discussion

6.1 Observed Contrast Ratio vs. PC-RVR Visibility – All Weather

The median CR values observed for measurements in the RVR reporting intervals for all three sets of lamps (HIRLs at 1,800', MALS at 1,800', and MALS at 2,400') are shown below. The median observed CR value for a particular lamp is plotted at the center of each RVR reporting bins, with lines connecting adjacent data points. No values are plotted for bins with inadequate sample size.

Although there were three PC-RVRs present and recording data, only the mid-field and 2,400' PC-RVR provided adequate data for analysis when correlated to contrast ratio measurements from the video. The tower PC-RVR had the least available raw data because of reduced reliability compared to the other two PC-RVRs. In addition, visual obstructions at AWRF frequently take the form of low-lying fog with a maximum altitude lower than that of the PC-RVR at the tower. Sufficient data points were only available for visibility in the 3,000-foot or higher bin, and as the results below show, those bins are less useful in evaluating the lamps.

The results in this section are summary results to compare the overall behavior of the lamps over the entire test campaign. As previously mentioned, it was infeasible for a human observer to review the many hours of camera and instrumentation data available. However, Appendix A provides the reader with some example stills taken from individual low-visibility events across a wide range of visibility and weather conditions and times of day.

6.1.1 HIRLs – 1,800’

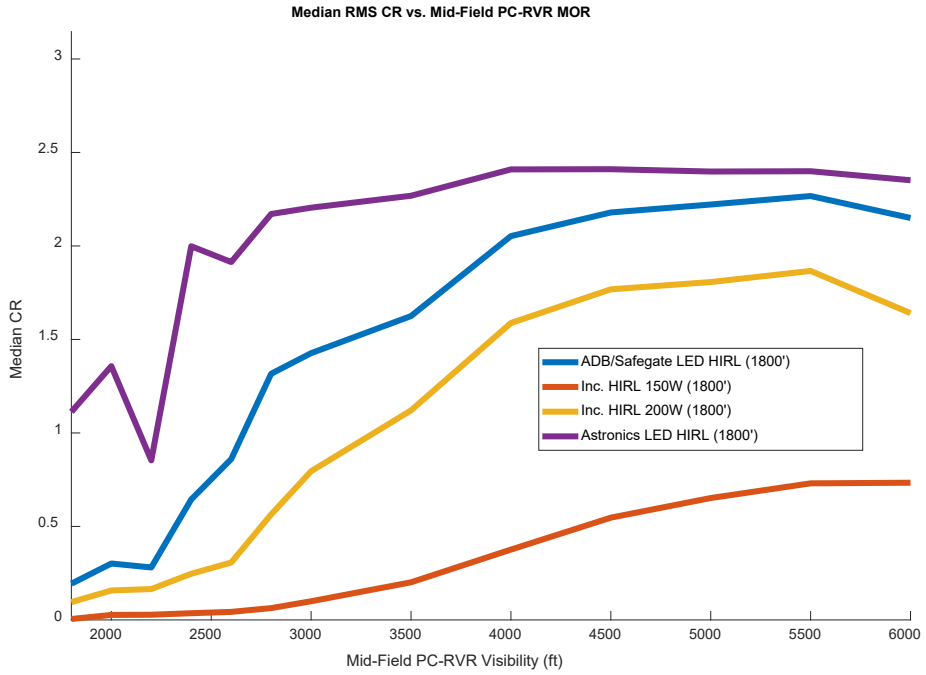

Figure 6-1: Observed CR vs. Mid-Field PC-RVR MOR, 1,800’ HIRLs

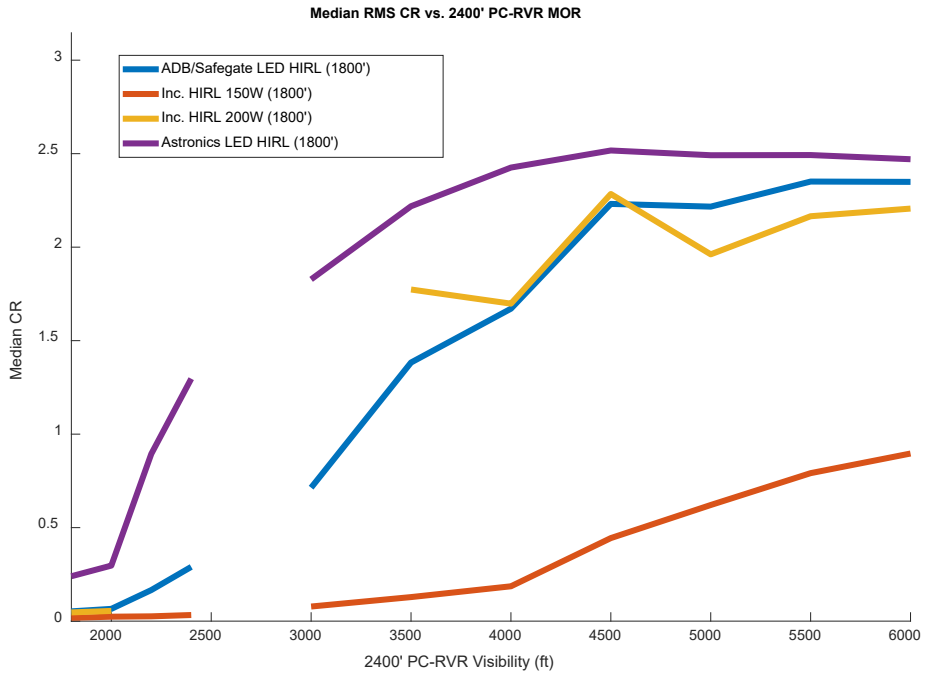

Figure 6-2: Observed CR vs. 2,400' PC-RVR MOR, 1,800’ HIRLs

The expected relationship between MOR and observed contrast ratio is evident in the data, with some scatter. Although the mid-field PC-RVR and the 2,400' PC-RVR are located approximately 1,000 feet apart, the median observed CR in each MOR bin, as reported by the two different instruments, is strikingly similar in trend. In absolute behavior, the CR of the lamps is generally higher at lower visibility when the mid-field measurement is used.

Using the mid-field PC-RVR as the reference instrument for visibility, there is a clear ordering of the lamps, with the Astronics LED lamp the brightest, the ADB/Safegate LED lamp second-brightest, and the 200W and 150W incandescent lamps substantially dimmer.

Using the 2400' PC-RVR as the reference instrument for visibility, the Astronics LED lamp is still clearly the brightest, but the ADB/Safegate and 200W incandescent lamps are of similar brightness, with the 150W incandescent lamp by far the dimmest.

One evident feature of the curves is that observed CR plateaus relatively rapidly with increasing MOR; more rapidly than might be expected. The fraction of remaining contrast $e^{-\frac{3.00}{MOR}X}$ predicted by Koschmieder's Law is only approximately 0.407 for the 1,800' row at an MOR of 6,000', while at 3,000' it is approximately 0.165. In other words, the observed CR should be more than twice as large at an MOR of 6,000' than 3,000'. This is close to the observed data for the dimmer lamps, but the brighter lamps appear to plateau around an MOR of 4,000', at a CR range of approximately 1.4 to 1.6.

This could reflect inadequate dynamic range in the camera given the shutter speed and aperture settings to capture the entire brightness change. If the apparent diameter of the lamp is constant and the portion of the sensor imaging the lamp becomes saturated (i.e. reports maximum light intensity), CR would remain constant even as actual received luminance increased.

6.1.2 MALS – 1,800’

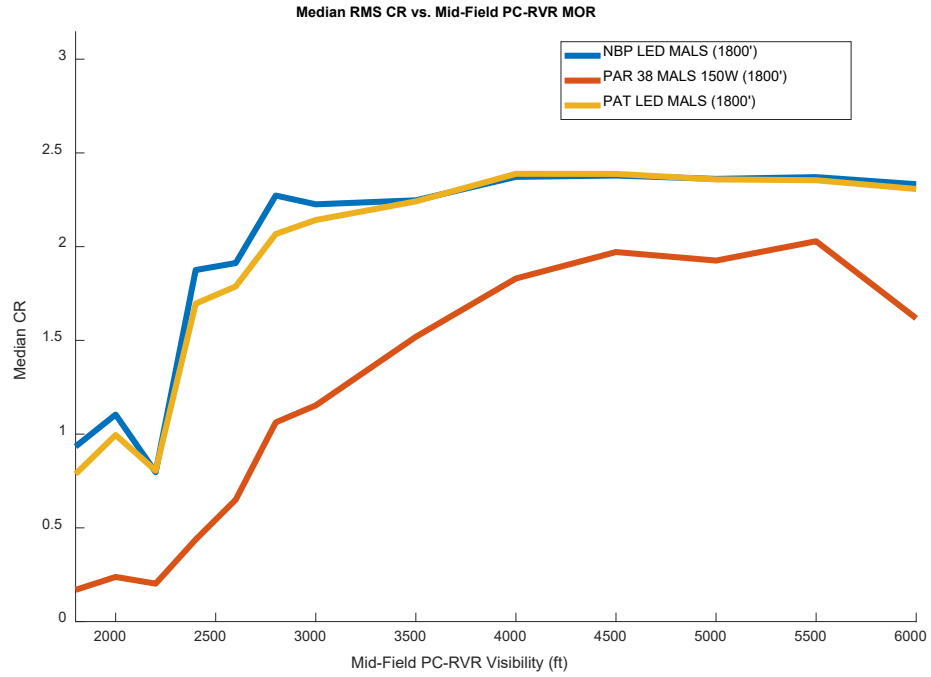

Figure 6-3: Observed CR vs. Mid-Field PC-RVR MOR, 1,800’ MALS

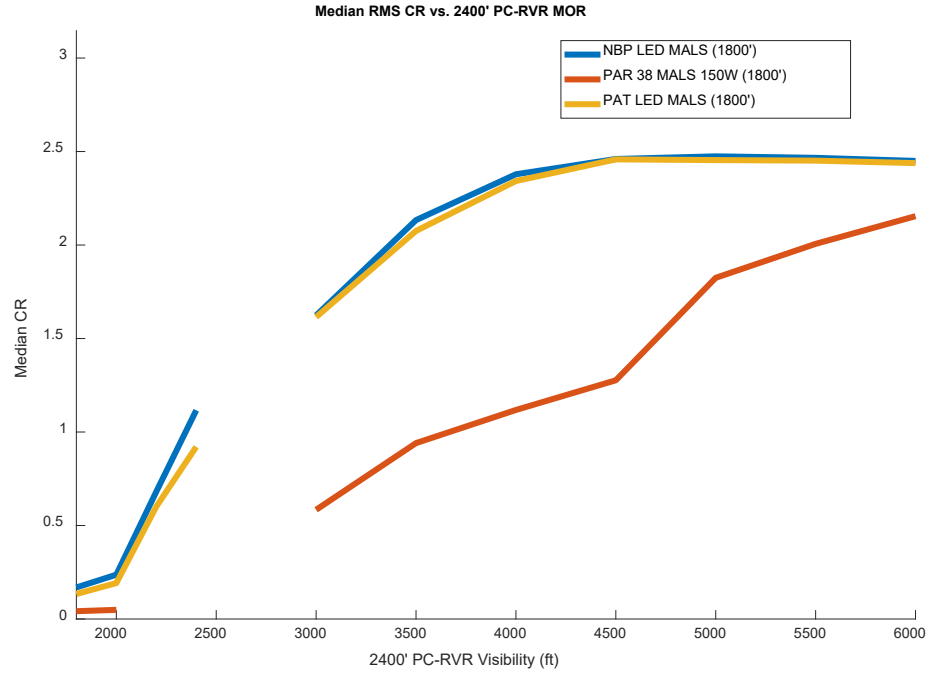

Figure 6-4: Observed CR vs. 2400' PC-RVR MOR, 1,800’ MALS

The expected relationship between CR and MOR is again evident, with the same features as observed for the 1,800' HIRLs. Using either the mid-field or 2,400' PC-RVR as the visibility reference, the NBP and Patriot LED lamps are essentially identical, while the nominally equivalent 150W PAR38 lamp is substantially dimmer. We again observe the plateau effect, with lamps again reaching a plateau at a CR of approximately 1.4 – 1.6; for the brightest lamps, this again corresponds to an MOR of approximately 4,000 feet.

6.1.3 MALS – 2,400’

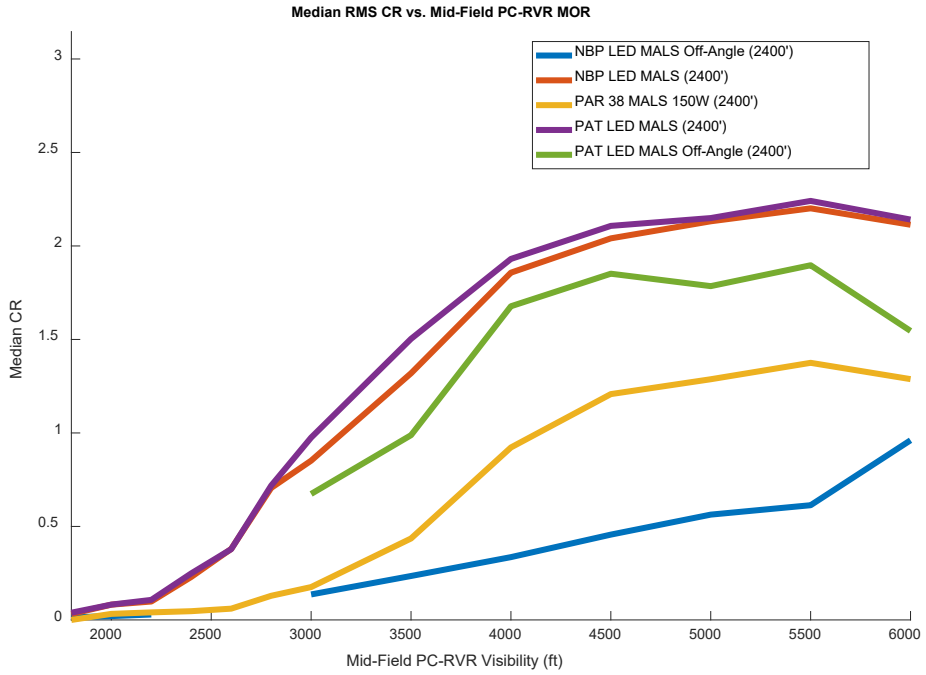

Figure 6-5: Observed CR vs. Mid-Field PC-RVR MOR, 2,400’ HIRLs

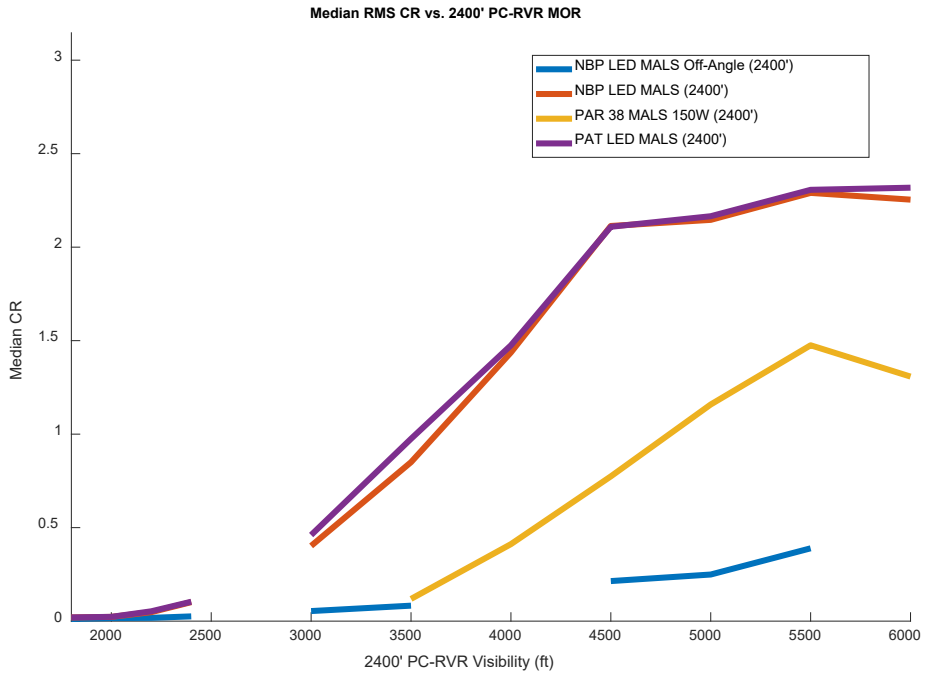

Figure 6-6: Observed CR vs. 2400’ PC-RVR MOR, 2,400’ HIRLs

We again see the expected relationship between CR and MOR. The observed CR values are similar regardless of the PC-RVR used as the visibility reference, with similar relative brightness ordering. The NBP and Patriot LED lamps are the brightest lamps and essentially identical; the off-angle Patriot LED lamp is slightly dimmer; the PAR38 150W incandescent lamp is substantially dimmer still, and the off-angle NBP LED lamp is by far the dimmest. The noticeable differences between the two off-angle LED lamps are more likely to be the result of different angles relative to the camera than actual brightness differences of the lamps, given the nearly-identical performance of the lamps that are oriented towards the camera.

6.2 Observed Contrast Ratio vs. PC-RVR Visibility – Fog, Rain, and Snow

In order to explore whether the relative behavior of LED and incandescent lamps varies based on weather type, the low-visibility events were divided into fog, rain, and snow event. As described in Section 4.2, the weather condition flags were not exclusive, in order to capture as much diverse weather data as possible. Because of the reduced number of observations available, the filtering process described in Section 5.7.3 was relaxed slightly, to require only 250 points in a bin to calculate a median value of CR. Other than this relaxed criterion, the analysis methodology was otherwise identical to the procedure used for the combined dataset.

To facilitate direct comparison between fog, rain, and snow results, the observed CR – MOR curves for each lamp are plotted in the same color, with fog results plotted with a solid line, rain results plotted with a dashed line, and snow results plotted with a dotted line. Most of the low-visibility data was collected in fog, so many of the rain and snow visibility bins have insufficient data to produce a median contrast ratio even after the number of required measurements was relaxed to 250.

6.2.1 HIRLs – 1,800’

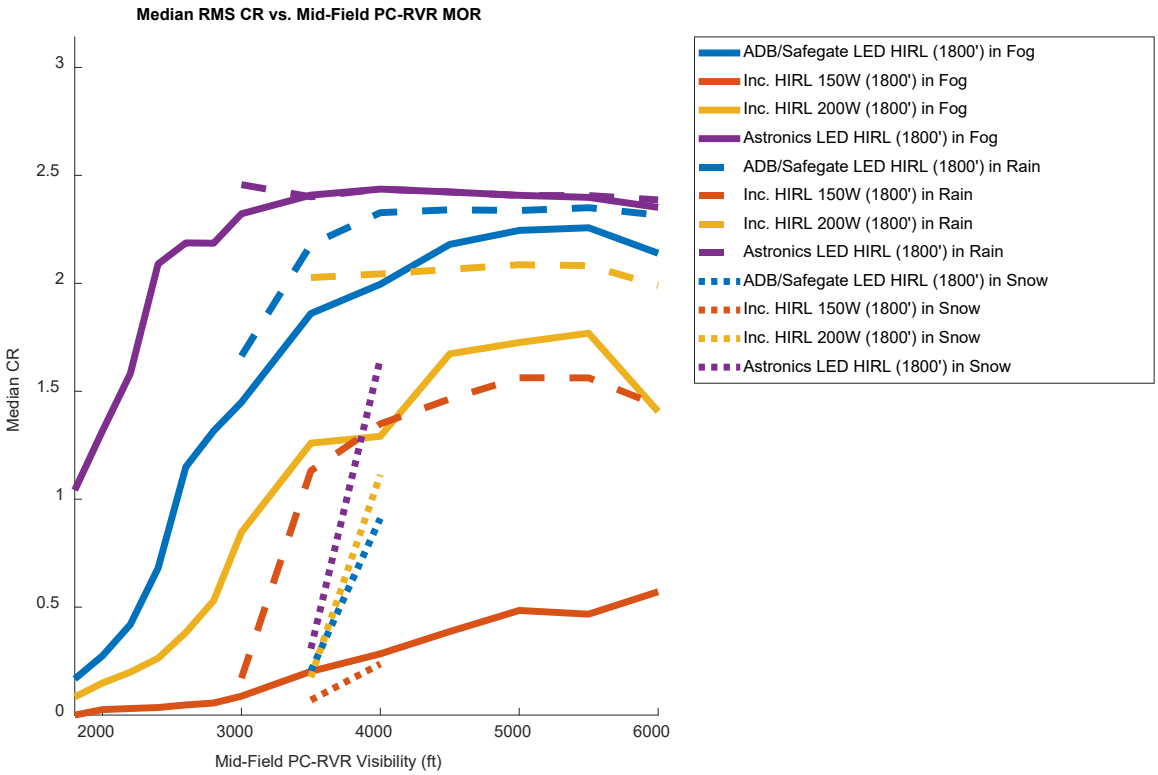

Figure 6-7: Observed CR vs. Mid-Field PC-RVR MOR, 1,800’ HIRLs in Fog/Rain/Snow

The observed CR – MOR relationship is very similar to what is observed with the entire dataset. It is evident that most of the low-visibility events are fog events, given the lack of data below about 3,000 feet visibility during rain, and the very little data available for snow. Both fog and rain have the same ordering from brightest to dimmest lamp, and that ordering agrees with the ordering using the entire dataset. The ordering for snow is slightly different, with the 200W incandescent HIRL and the ADB/Safegate HIRL switching places, but more data would be required to determine if there really is a difference in snow.

One interesting feature revealed by separating out fog and rain events is that the lamps are easier to distinguish (i.e. have a larger contrast ratio) during rain than they are during fog at the same measured MOR. This is likely attributable to a feature of forward-scatter-meters like the PC-RVR sensors; namely, that they can underestimate visibility in rain compared to human observers or human-observer-like instruments (e.g. transmissometers) by as much as a factor of two (Waas, 2008). In other words, if the PC-RVR reports a visibility of 3,000 feet during rain, the true visibility might be as much as 6,000 feet.

Since the camera-based test setup has similarities to a transmissometer (although its properties and the

overall lamp brightness stability were not designed for this purpose), it is likely that the camera is more accurately reporting the "true" visibility in the form of a significantly higher CR than would be expected based on the reported visibility from a PC-RVR.

Unlike during rain, the reported contrast ratios for the lamps are considerably lower in snow than in either fog or rain. Because of the lack of data, it is not possible to draw strong conclusions, but the differences may partly be due to reduced contrast between a bright lamp and white, snow-covered surroundings. Reviewing some of the snow-event footage confirms that it can be very challenging to distinguish the lamps from surrounding snow, particularly during the daytime, when the lamps tend to blend in with their surroundings. Appendix A shows examples of frames collected during low- and moderate-visibility periods of snow.

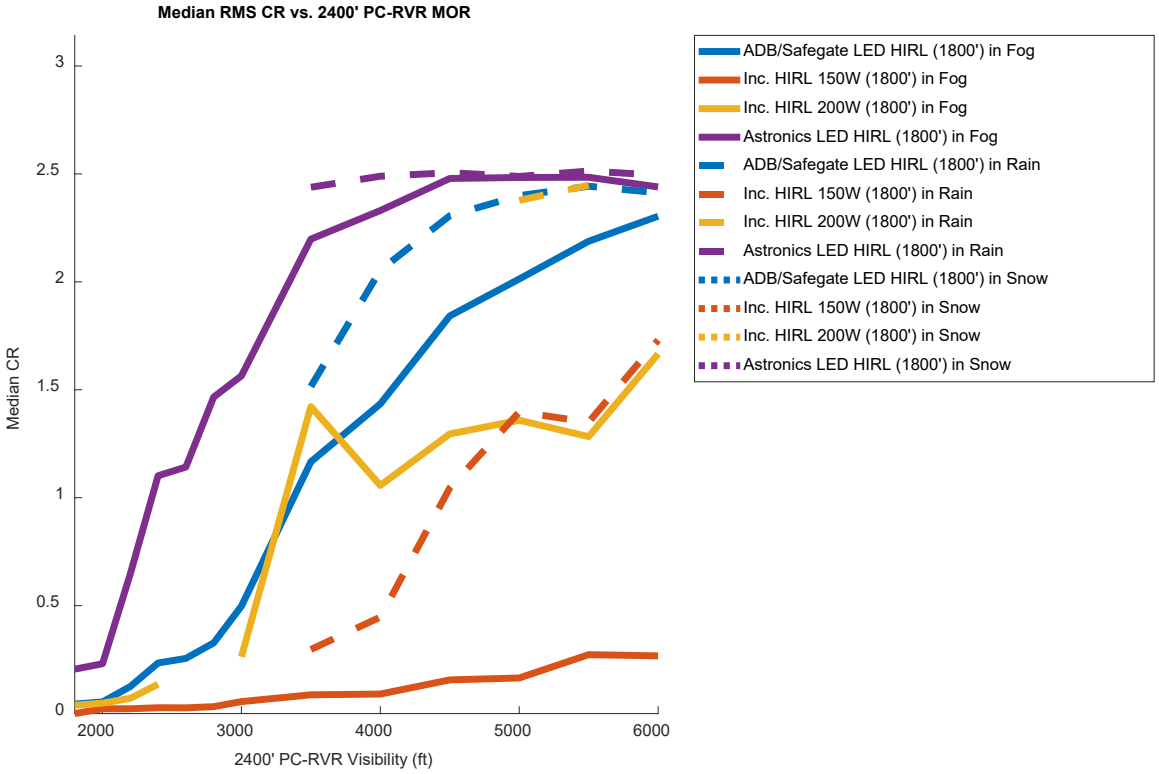

Figure 6-8: Observed CR vs. 2400' PC-RVR MOR, 1,800’ HIRLs in Fog/Rain/Snow

The observed CR – MOR relationship is again very similar to what is observed with the entire dataset. Both fog and rain have the same ordering from brightest to dimmest lamp, and it agrees with the ordering using the entire dataset. We again see the phenomenon that the observed CR is substantially higher for rain than fog at the same MOR. Unfortunately, the reduced data available from the 2,400’ PC-RVR and the small number of snow events means there is no information about median CR values in snow for any of the lamps.

6.2.2 MALS – 1,800’

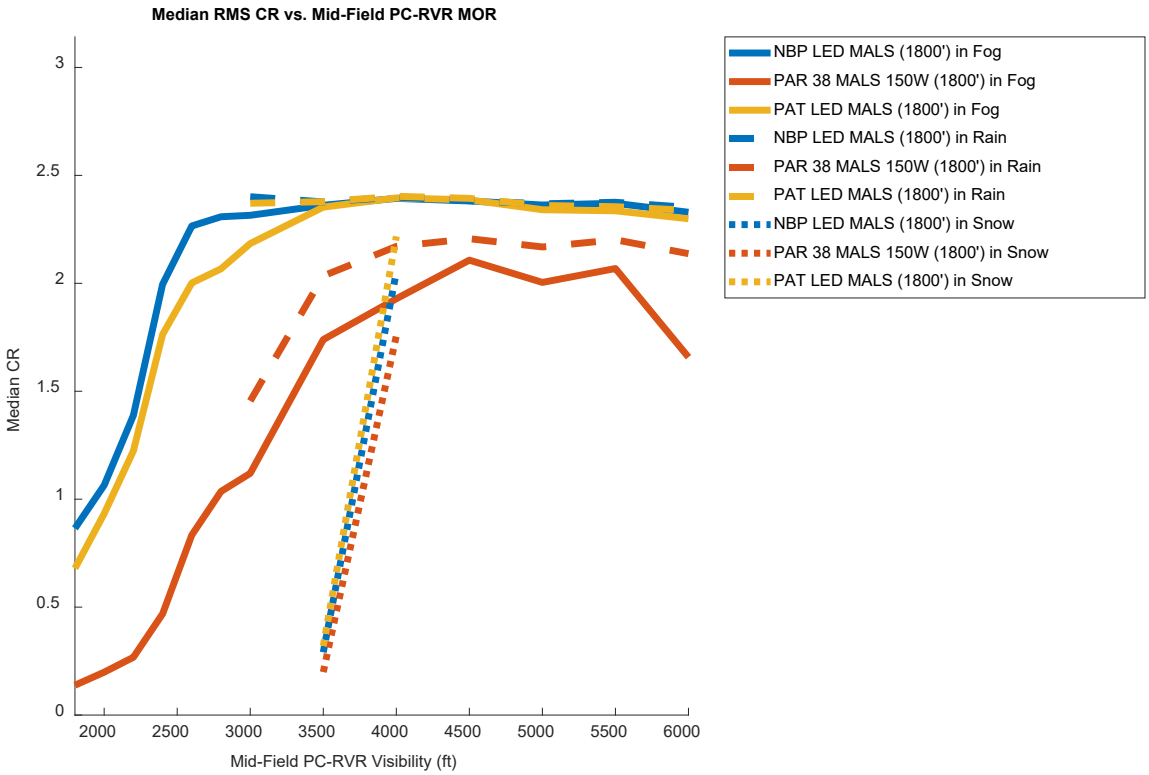

Figure 6-9: Observed CR vs. Mid-Field PC-RVR MOR, 1,800’ MALS in Fog/Rain/Snow

The same behavior is present here as with the 1,800’ HIRLs: the same relative behavior is observed between rain and fog, but observed CR is higher in rain than fog. In this case, the snow also preserves the same relative ordering as the rain and fog measurements. For these lamps, we again observe a lower CR associated with the same measured MOR during snow events. The difference between fog and rain is less substantial here than for the HIRLs, likely because the higher inherent contrast of the lamps means they are plateaued for more of the visibility range.

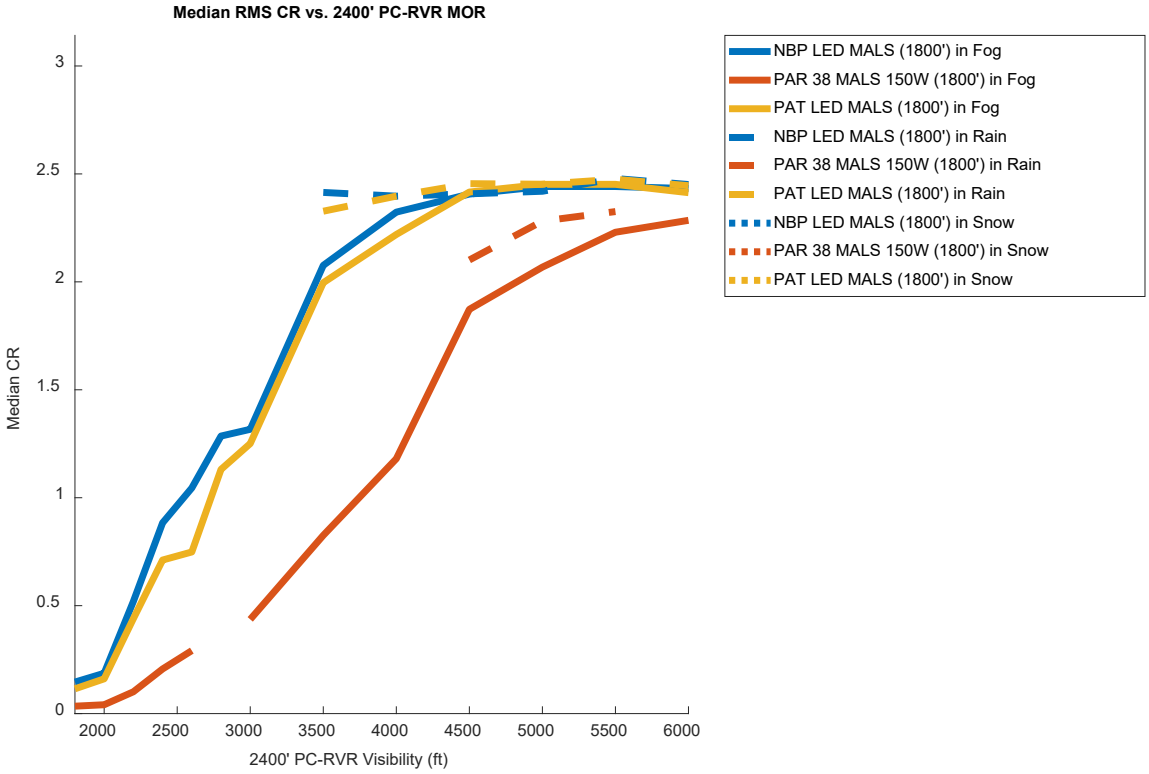

Figure 6-10: Observed CR vs. 2,400' PC-RVR MOR, 1800' MALS in Fog/Rain/Snow

The same behavior is present here as with the 1,800' HIRLs: the same relative behavior is observed between rain and fog, but observed CR is higher in rain than fog. We again have no snow data because of the reduced amount of visibility data available from the 2,400' PC-RVR and the relative lack of snow events.

6.2.3 MALS – 2,400’

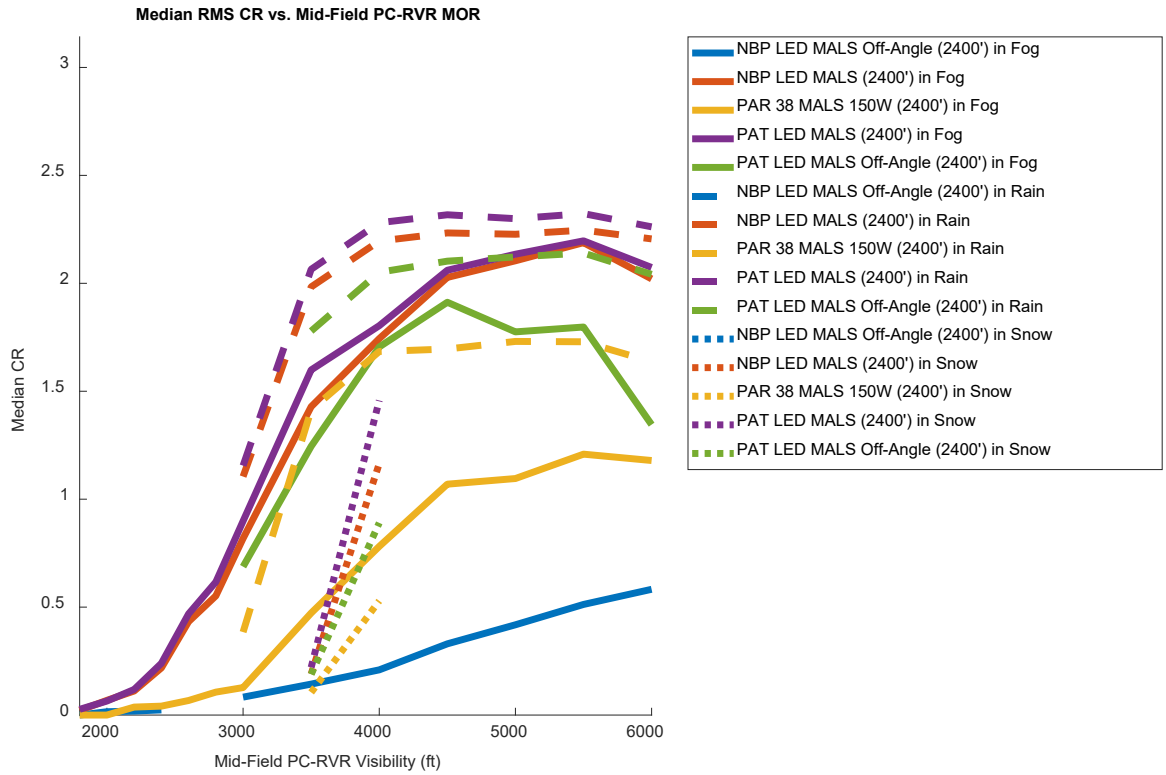

Figure 6-11: Observed CR vs. Mid-Field PC-RVR MOR, 2,400’ MALS in Fog/Rain/Snow

The same behavior is present here as with the other sets of lamps: the same relative behavior is observed between rain and fog, but observed CR is higher in rain than fog. Snow again preserves the relative ordering, but with a substantially lower CR value at the same PC-RVR MOR.

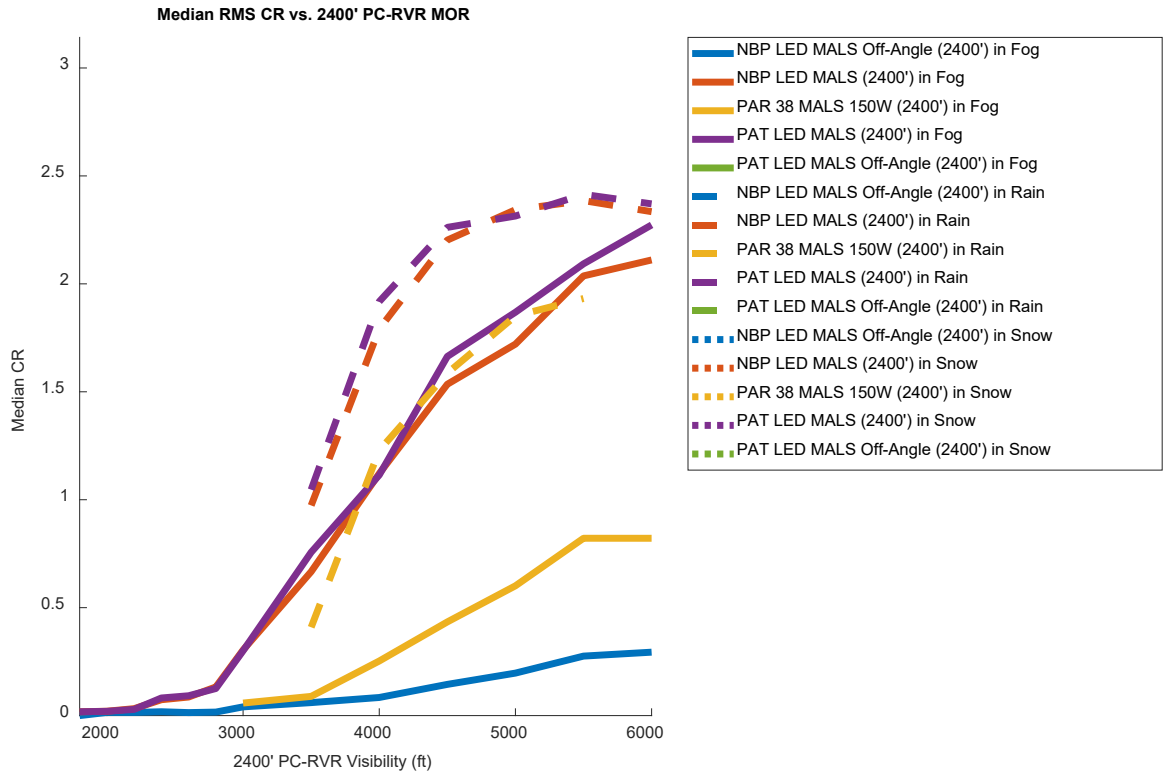

Figure 6-12: Observed CR vs. 2,400’ PC-RVR MOR, 2,400’ MALS

The same behavior is present here as with the other sets of lamps: the same relative behavior is observed between rain and fog, but observed CR is higher in rain than fog. Note that the off-angle Patriot LED generally does not have enough data, when separated out into fog and rain, to pass the reduced data count criterion. We also lack enough data collected in snow to show any results for this combination of visibility source and lamps.

7. Conclusions

Despite the challenges associated with turning a qualitative data-collection effort into a quantitative analysis effort, the analysis was successful. We were able to leverage the large quantity of data collected over the course of the experiment to assess the relative brightness of the LED lamps to their incandescent counterparts.

The observed relationship between contrast ratio and visibility agrees well with the Koschmieder's Law relationship, validating the RMS contrast ratio metric applied here as a valid proxy for the subjective brightness experienced by human observers. The results of the testing and analysis conclusively demonstrate that, at maximum intensity, LED lamps are substantially easier to see than the standard incandescent lamps they are nominally designed to replace. This behavior is consistent across all periods of reduced visibility observed during the data collection, regardless of the weather conditions causing the reduced visibility.

The improvement in brightness of the LED lamps over the incandescent lamps are particularly striking at measured visibility values comparable to the distance from the camera to the lamps. In these conditions, where the RVR measurement indicates the lamps should be just barely distinguishable from their backgrounds, it was typical for the incandescent lamps to be either barely visible or indistinguishable from the background, while the equivalent LED lamps would generally still be easily recognizable as lamps.

One possible opportunity revealed by the data collection effort and subsequent analysis is the potential application of a relatively inexpensive system employing a visible-spectrum camera to the measurement of visibility by refining the techniques used in this study. Many low volume and/or remote airports in the United States and elsewhere have established lighting infrastructure for use in night operations, but do not have visibility-measuring equipment. A visual-spectrum camera, with knowledge of the inherent contrast of a lamp (i.e. the contrast ratio associated with a particular brightness setting in high-visibility conditions) could conceivably be installed facing already-existing lighting infrastructure to provide an estimate of visibility.

8. References

Local luminance and contrast in natural images. **Frazor, Robert A. and Geisler, Wilson S. 2006.** 10, s.l. : Elsevier, 2006, Vol. 46, pp. 1585-1598.

Matching LED and Incandescent Aviation Signal Brightness. **Bullough, John D. 2014.** Galloway, NJ : FAA Worldwide Airport Technology Transfer Conference, 2014.

Measuring Contrast Sensitivity. **Pelli, Denis G. and Bex, Peter. 2013.** s.l. : Elsevier, September 20, 2013, Vision Research, Vol. 90, pp. 10-14.

Pattison, Paul M, Hansen, Monica and Tsao, Jeffrey Y. 2018. LED lighting efficacy: Status and directions. *Comptes Rendus Physique.* s.l. : Elsevier, 2018. Vol. 19, 3. ISSN 1631-0705.

Waas, Stefan. 2008. *Field Test of Forward Scatter Meter Visibility Sensors at German Airports.* Hamburg : German Meteorological Service (DWD), 2008.

Appendix A: Example Photographs under Various Weather Conditions

Low Visibility (Visibility ≤ 1,800')

Dawn

Fog

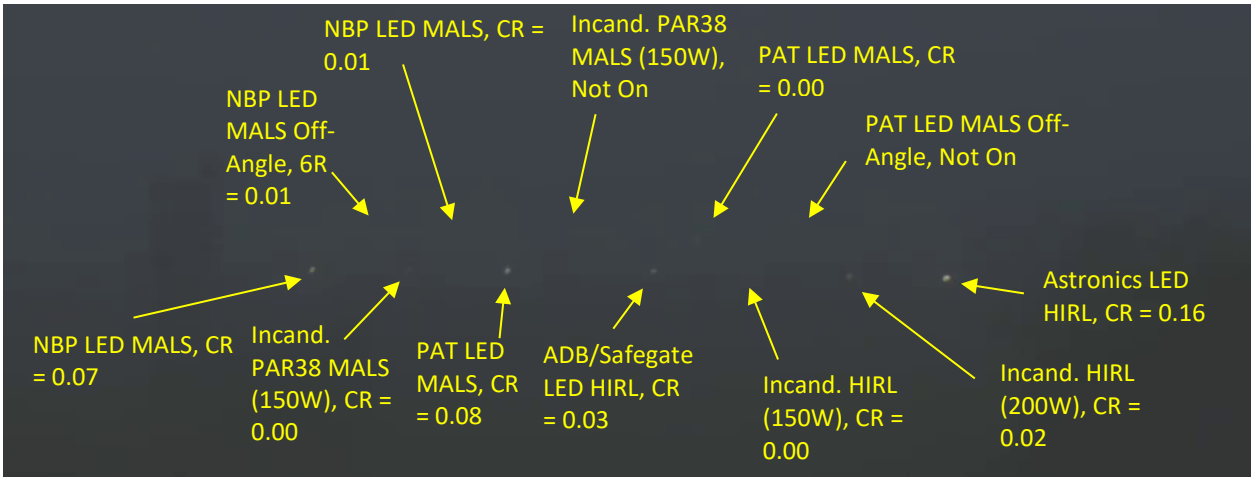

Figure A-1: June 27, 2019 at 0538 hrs

Image date and time: June 27, 2019 at 5:38 AM
Approximate visibility: 1,500'
METAR weather code: FG

Rain

No example available.

Snow

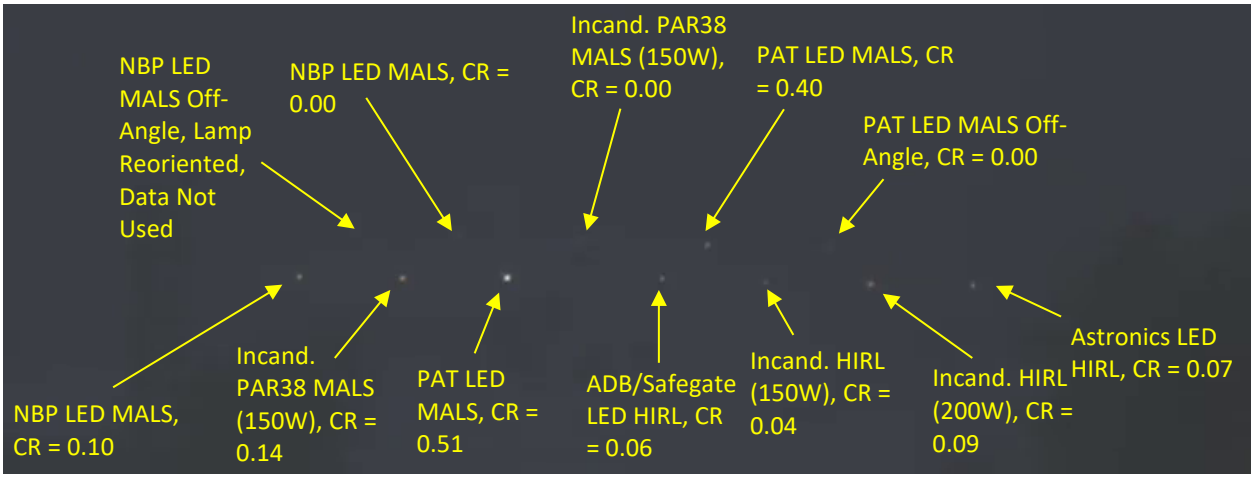

Figure A-2: December 3, 2019 at 0735 hrs

Image date and time: December 3, 2019 at 7:35 AM
Approximate visibility: 1,800'
METAR weather code: -SN

Day

Fog

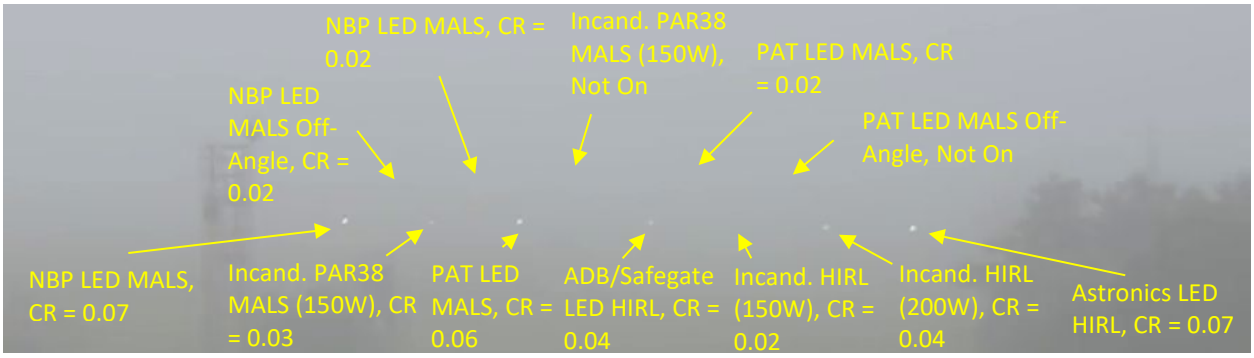

Figure A-3: June 20, 2019 at 1011 hrs

Image date and time: June 20, 2019 at 10:11 AM
Approximate visibility: 1,800'
METAR weather code: FG

Rain

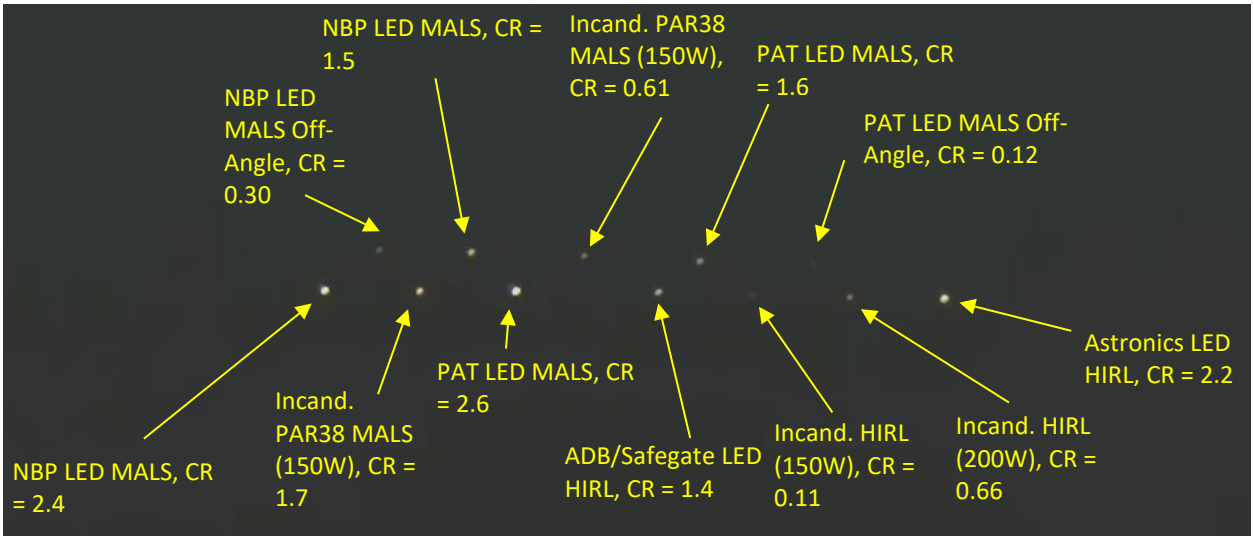

Figure A-4: July 23, 2019 at 1125 hrs

Image date and time: July 23, 2019 at 11:25 AM[4]
Approximate visibility: 1,300'
METAR weather code: +RA

[4] Although the extremely low visibility makes the image very dark, the time is correct. The video shows a normal daylight scene once the low-visibility event ends.

Snow

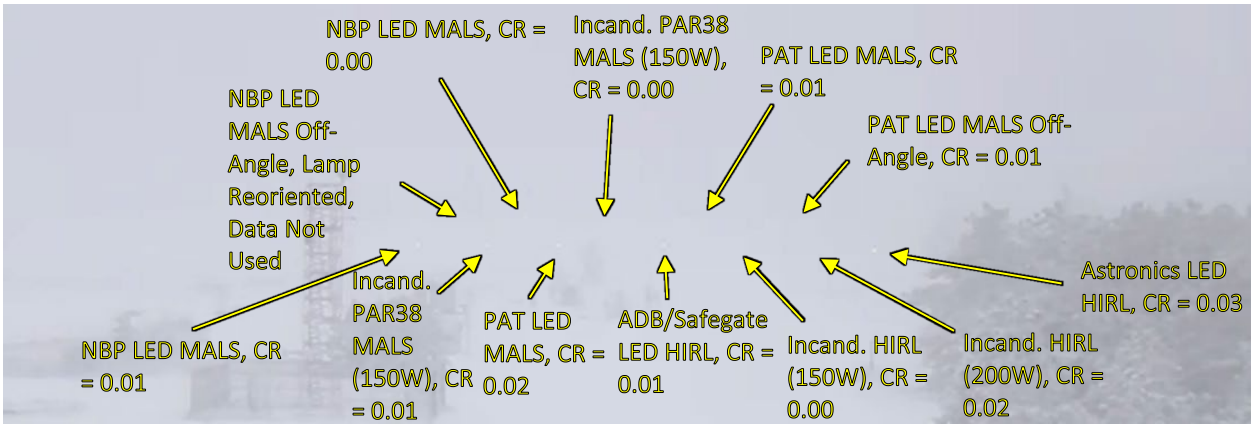

Figure A-5: December 3, 2019 at 1156 hrs

Image date and time: December 3, 2019 at 11:56 AM
Approximate visibility: 1,600'
METAR weather code: -SN

Dusk

Fog

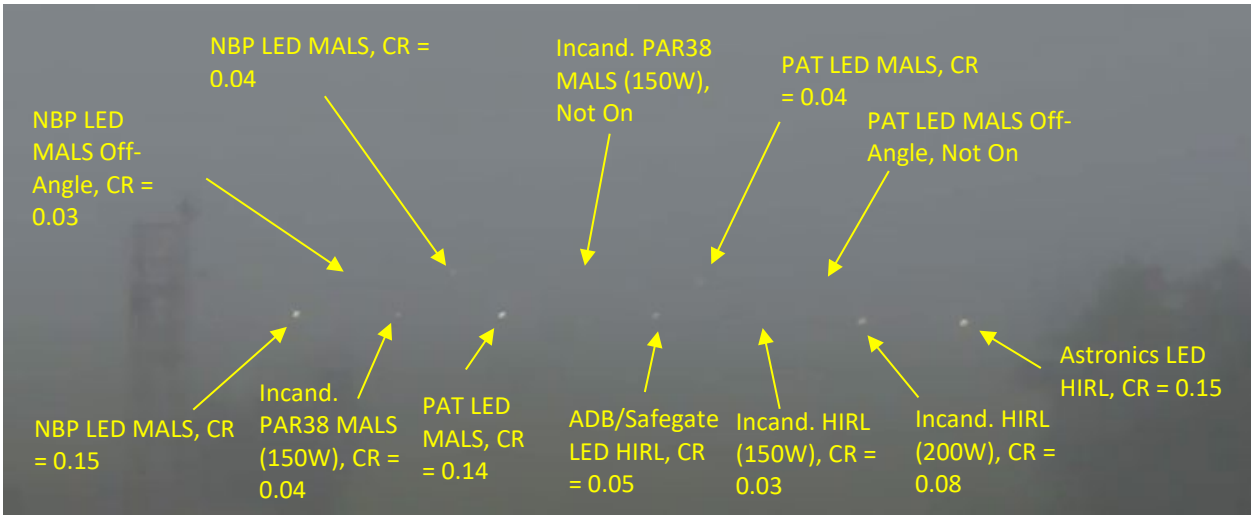

Figure A-6: June 20, 2019 at 1800 hrs

Image date and time: June 20, 2019 at 6:00 PM
Approximate visibility: 1,800 feet
METAR weather code: FG

Rain

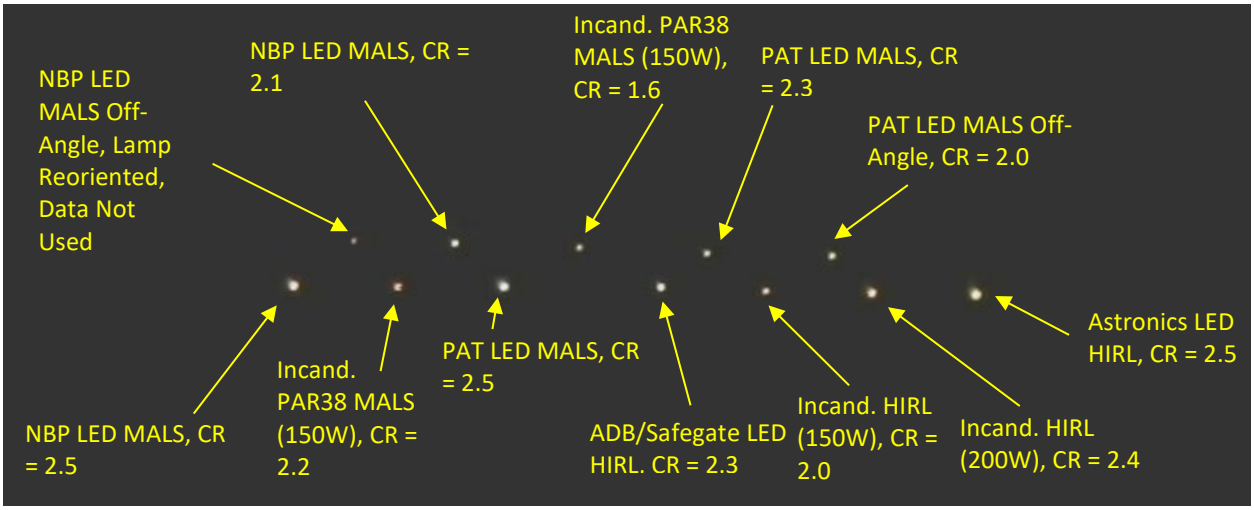

Figure A-7: October 27, 2019 at 1803 hrs

Image date and time: October 27, 2019 at 6:03 PM
Approximate visibility: 1,800'
METAR weather code: -RA BR

Snow

No example available.

Night

Fog

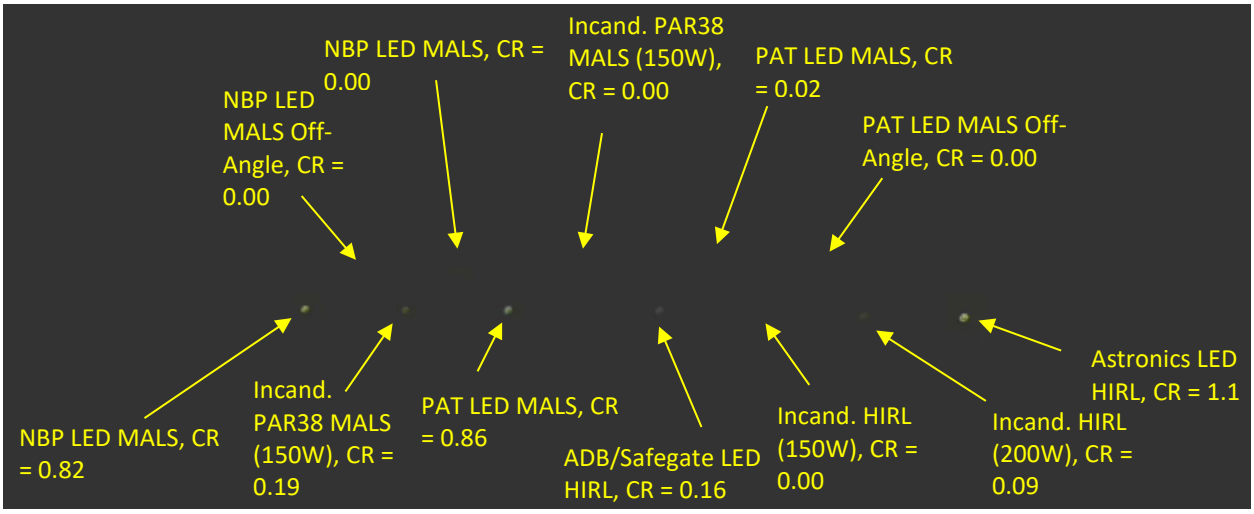

Figure A-8: July 19, 2019 at 2210 hrs

Image date and time: July 19, 2019 at 10:10 PM
Approximate visibility: 1,500 feet
METAR weather code: BR

Rain

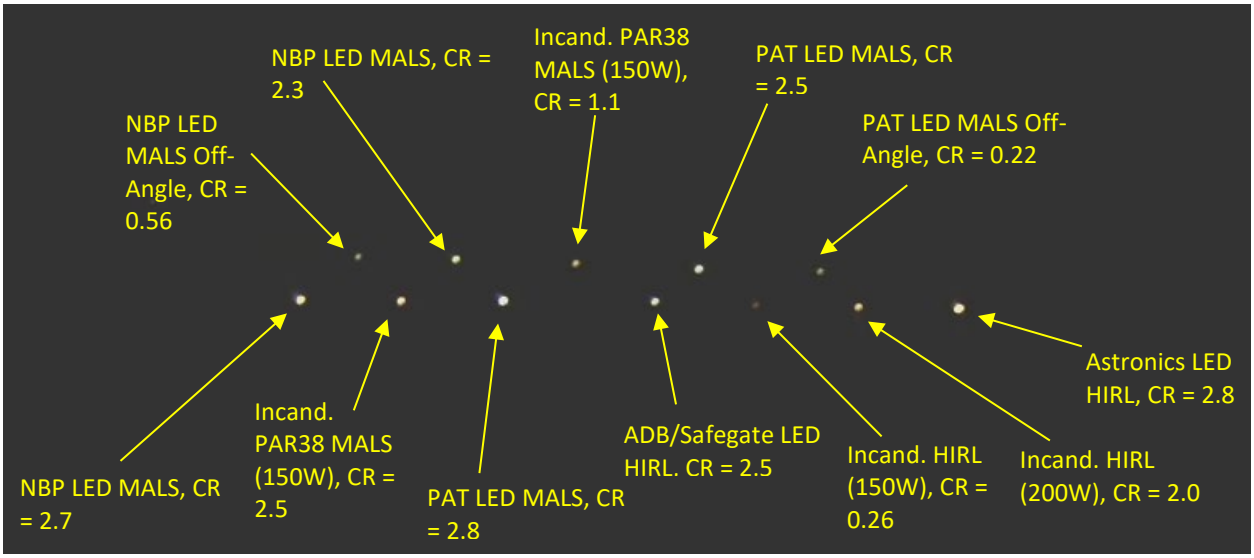

Figure A-9: July 18, 2019 at 2135 hrs

Image date and time: July 18, 2019 at 9:35 PM
Approximate visibility: 1,500 feet
METAR weather code: +RA

Snow

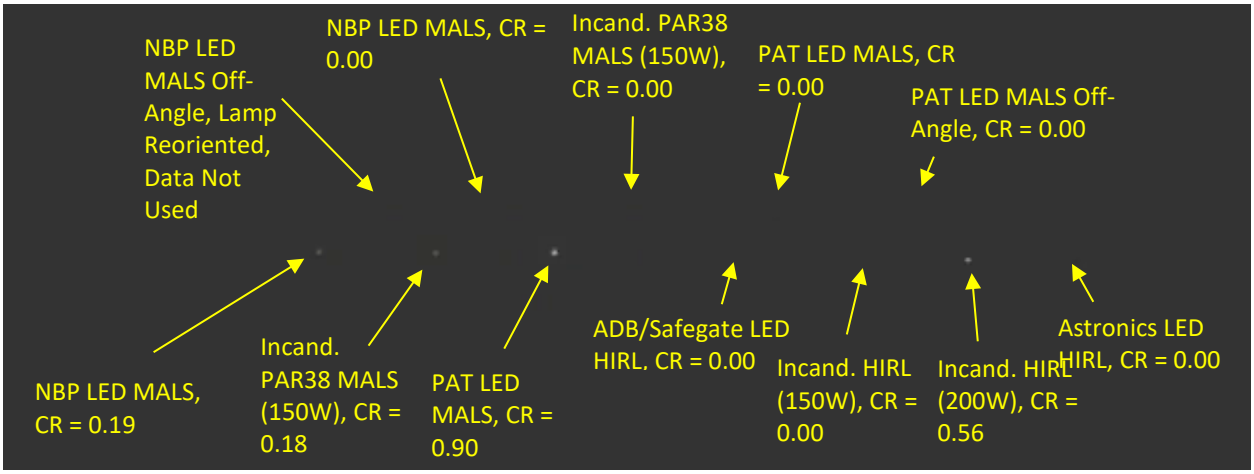

Figure A-10: Jan 8, 2020 at 0105 hrs

Image date and time: Jan 8, 2020 at 1:05 AM
Approximate visibility: 1,600’
METAR weather code: -SN

Moderate Visibility (3,000’ ≤ Visibility ≤ 6,000’)

Dawn

Fog

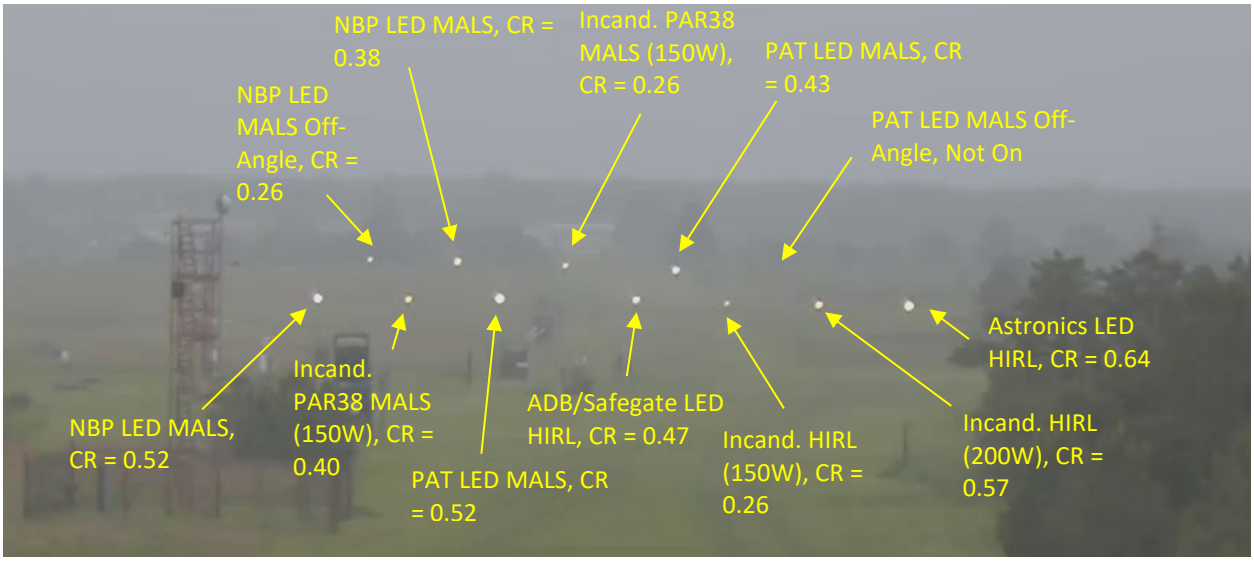

Figure A-11: June 14, 2019 at 0705 hrs

Image date and time: June 14, 2019 at 7:05 AM
Approximate visibility: 5,500’
METAR weather code: BR

Rain

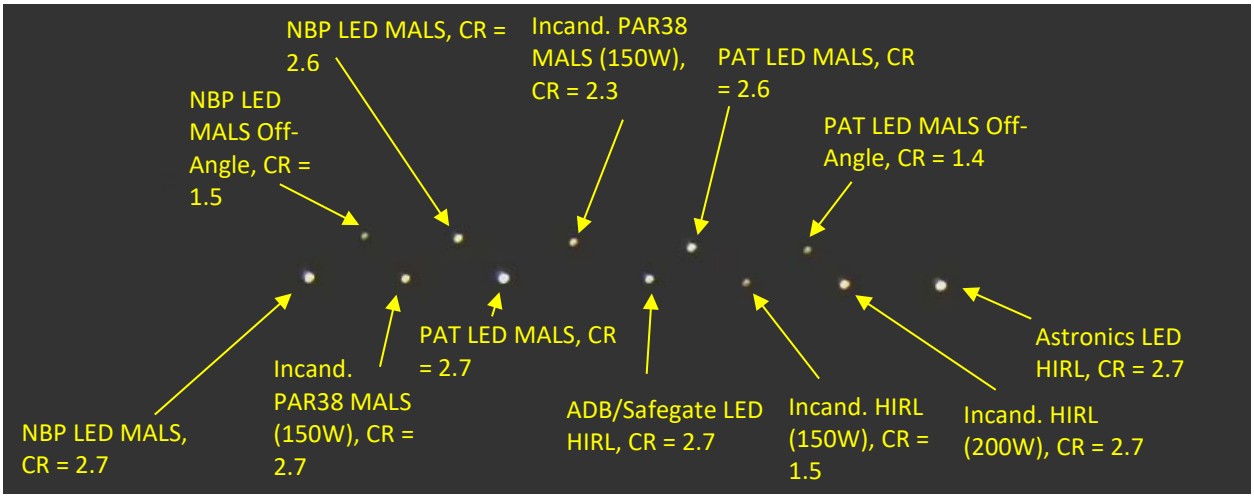

Figure A-12: August 29, 2019 at 0607 hrs

Image date and time: August 29, 2019 at 6:07 AM
Approximate visibility: 3,000'
METAR weather codes: TS RA

Snow

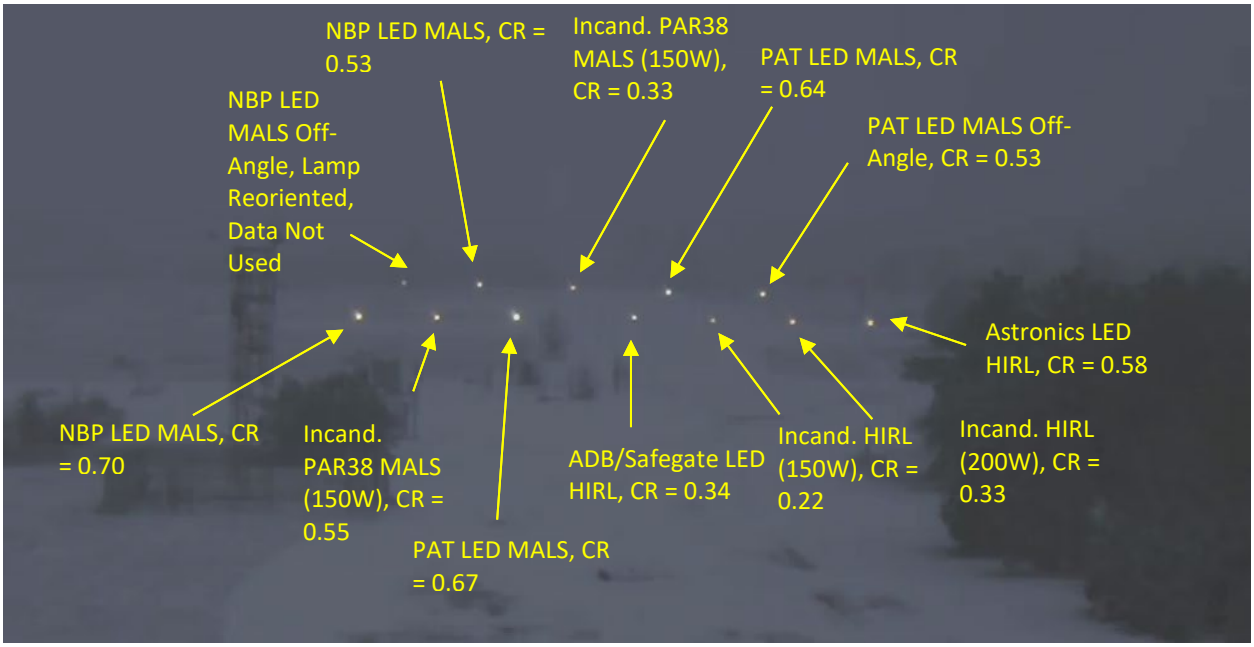

Figure A-13: December 3, 2019 at 0750 hrs

Image date and time: December 3, 2019 at 7:50 AM
Approximate visibility: 6,000'
METAR weather code: -SN

Day

Fog

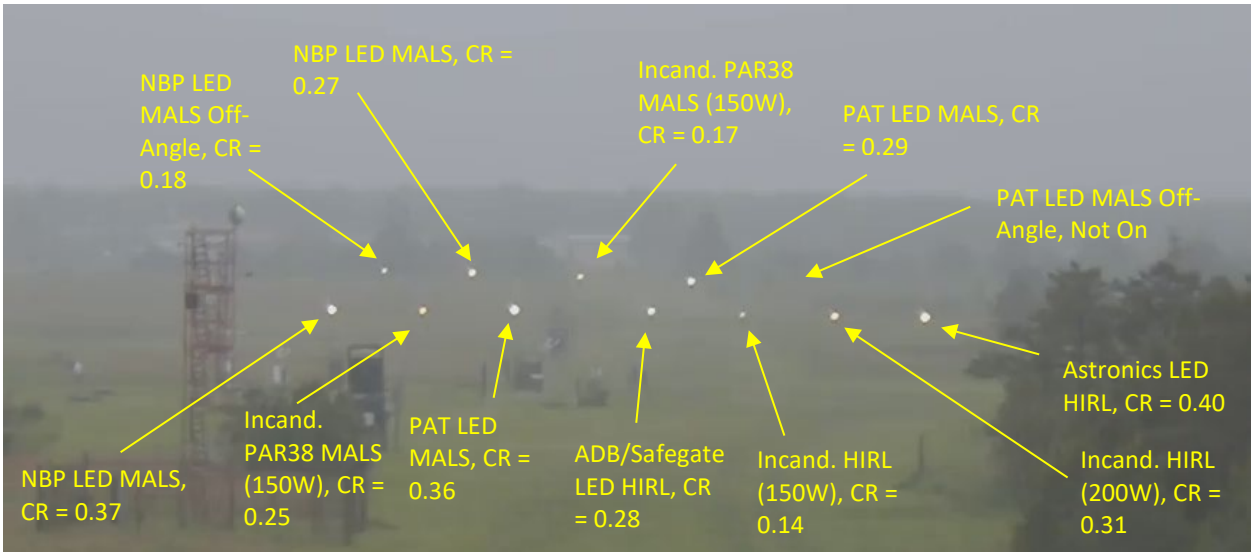

Figure A-14: June 13, 2019 at 1125 hrs

Image date and time: June 13, 2019 at 11:25 AM
Approximate visibility: 5,000'
METAR weather code: BR

Rain

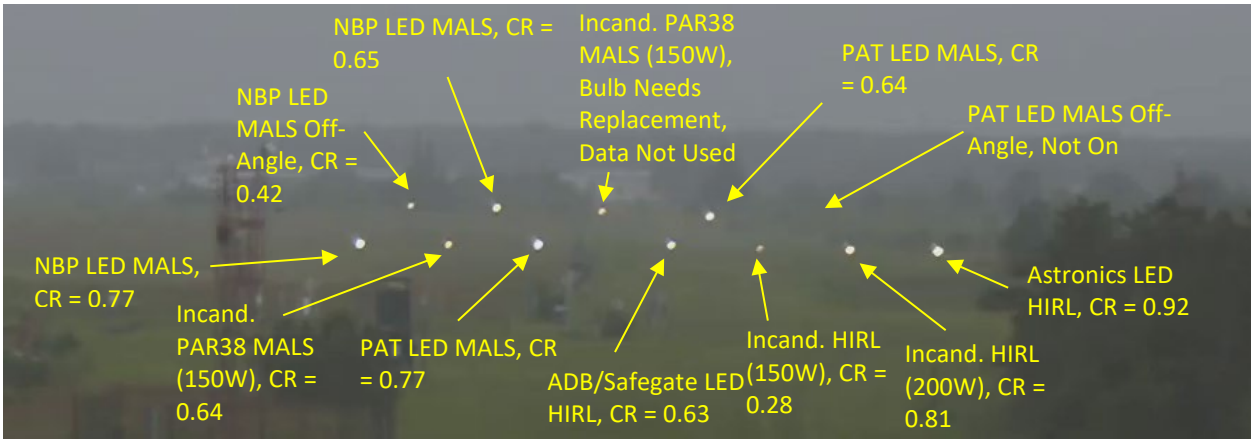

Figure A-15: June 20, 2019 at 0805 hrs

Image date and time: June 20, 2019 at 8:05 AM
Approximate visibility: 6,000'
METAR weather code: RA

Snow

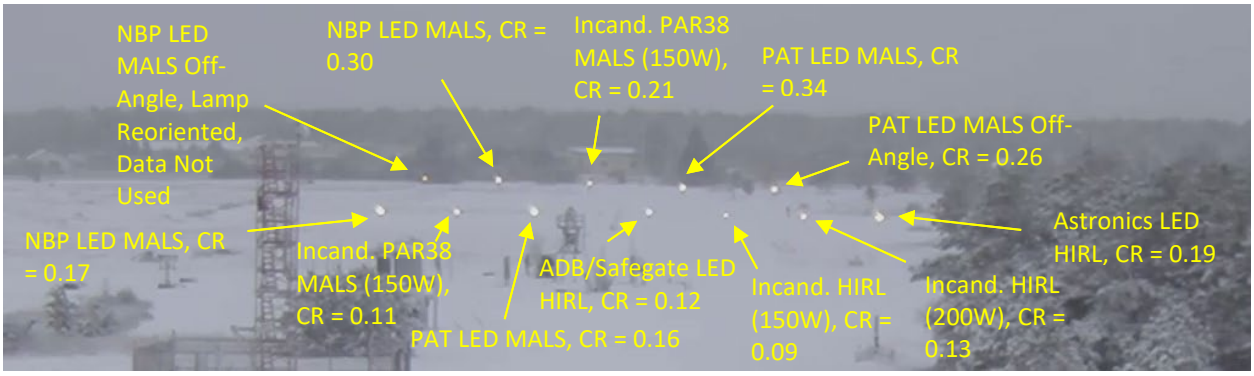

Figure A-16: December 3, 2019 at 1300 hrs

Image date and time: December 3, 2019 at 1:00 PM
Approximate visibility: 6,000'
METAR weather code: -SN

Dusk

Fog

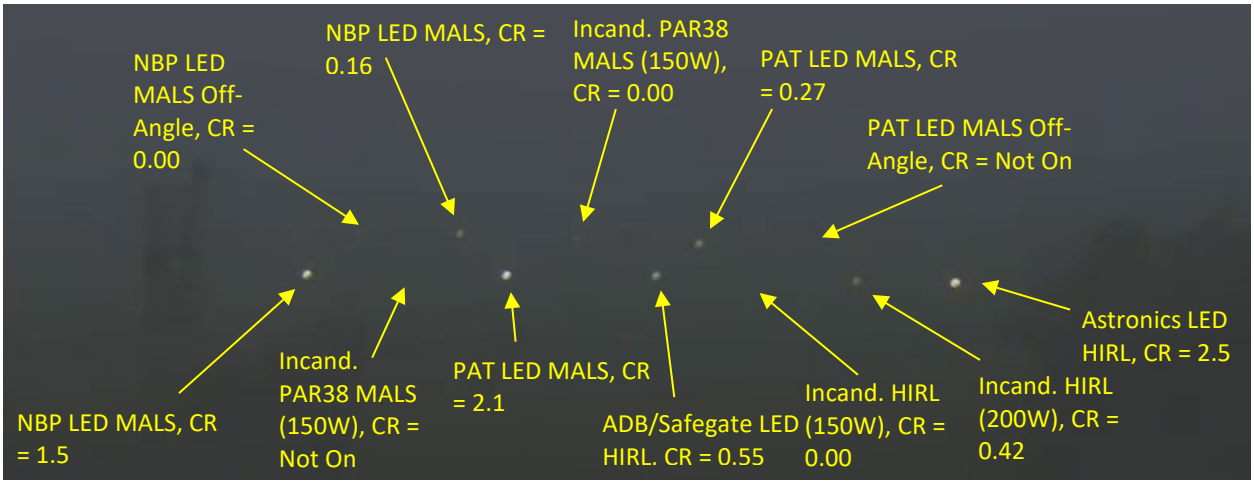

Figure A-17: July 6, 2019 at 1847 hrs

Image date and time: July 6, 2019 at 6:47 PM
Approximate visibility: 3,300 feet
METAR weather code: FG

Rain

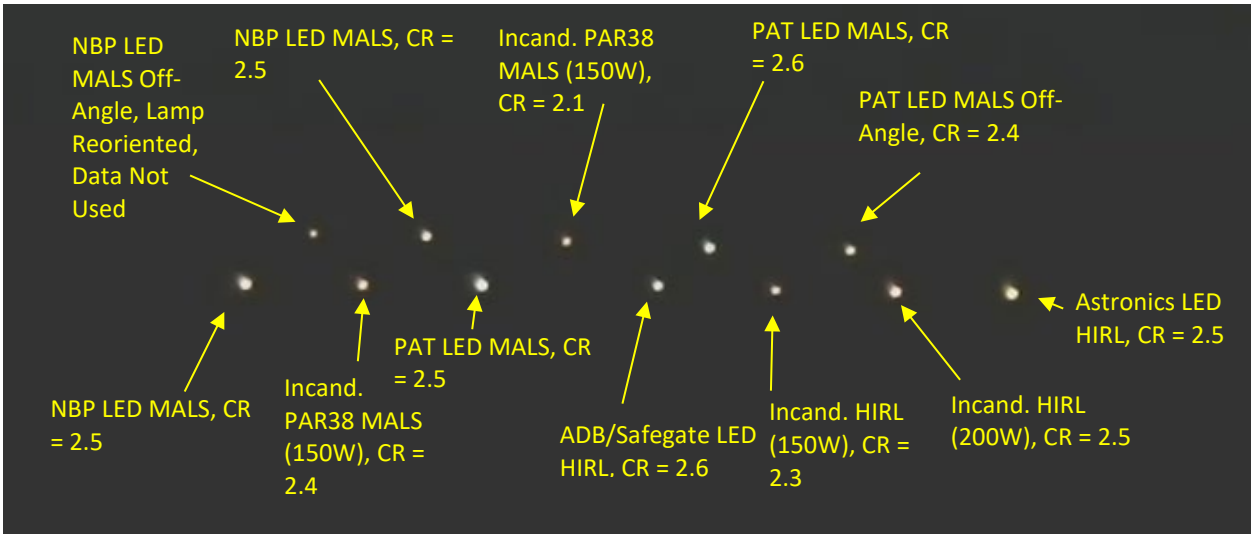

Figure A-18: October 27, 2019 at 1735 hrs

Image date and time: October 27, 2019 at 5:35 PM
Approximate visibility: 6,000'
METAR weather code: -RA BR

Snow

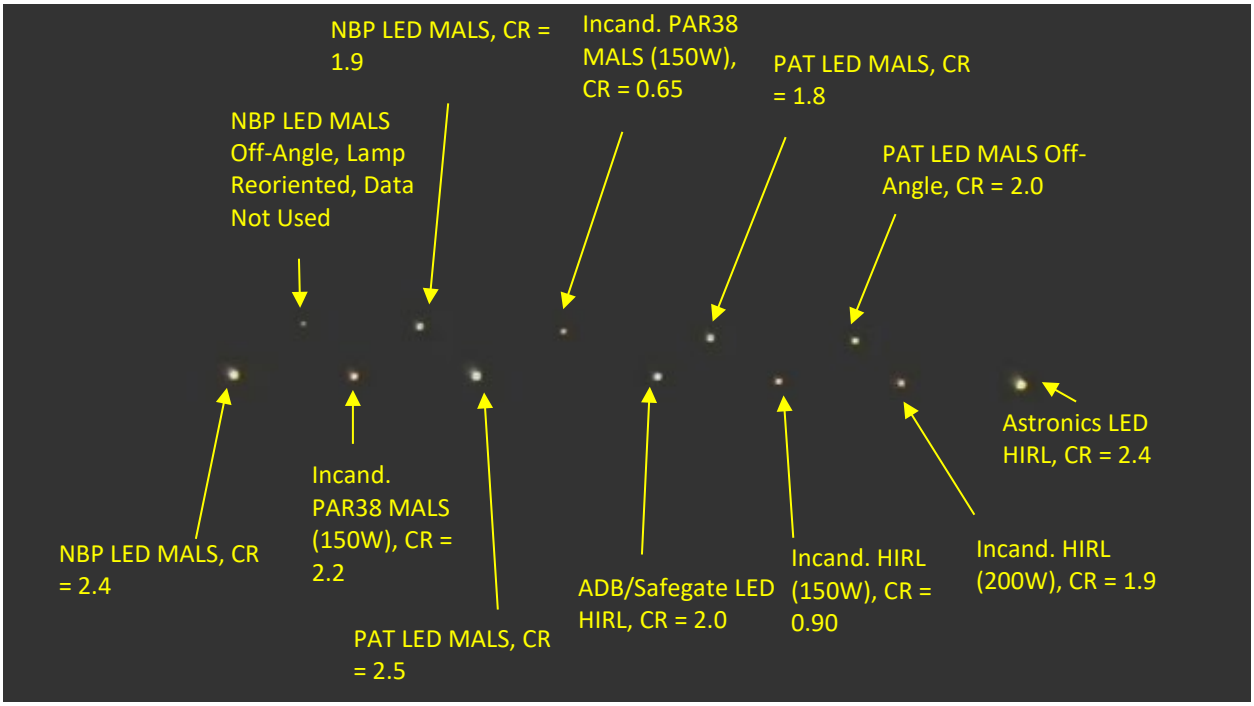

Figure A-19: November 12, 2019 at 1640 hrs

Image date and time: November 12, 2019 at 4:40 PM
Approximate visibility: 3,500'
METAR weather code: -SN

Night

Fog

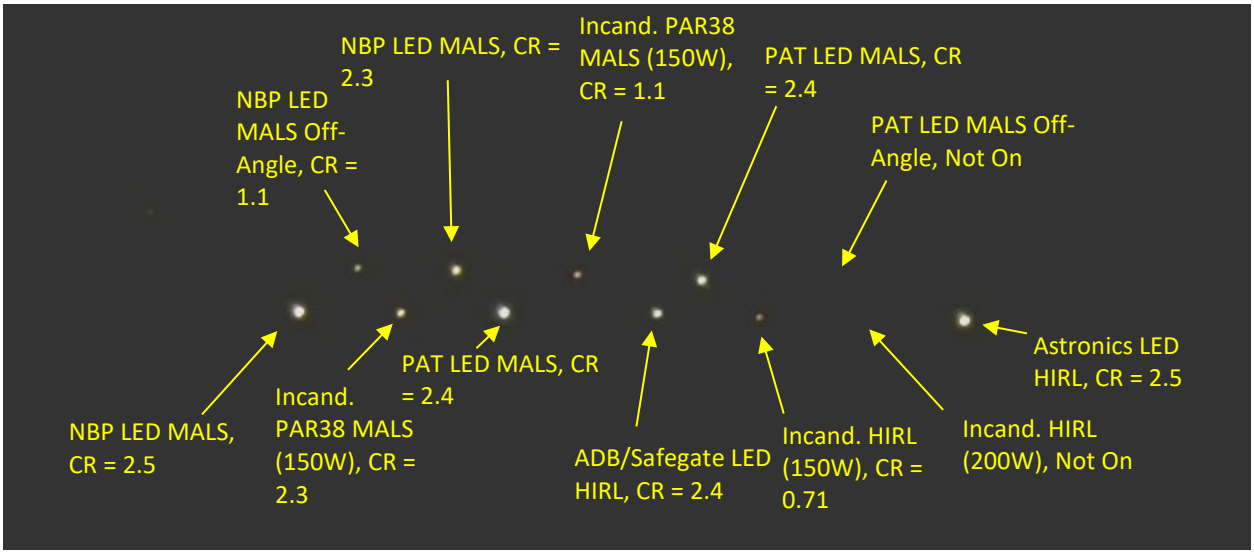

Figure A-20: May 31, 2019 at 0245 hrs

Image date and time: May 31, 2019 at 2:45 AM
Approximate visibility: 6,000’
METAR weather code: BR

Rain

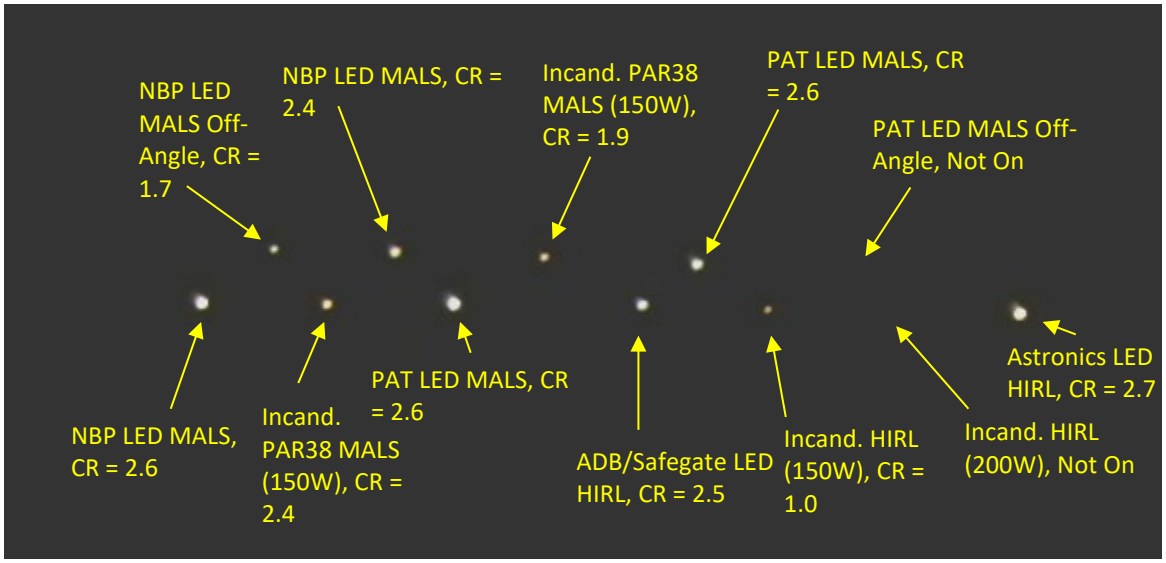

Figure A-21: May 30, 2019 at 0000 hrs

Image date and time: May 30, 2019 at 12:00 AM
Approximate visibility: 6,000'
METAR weather code: -DZ

Snow

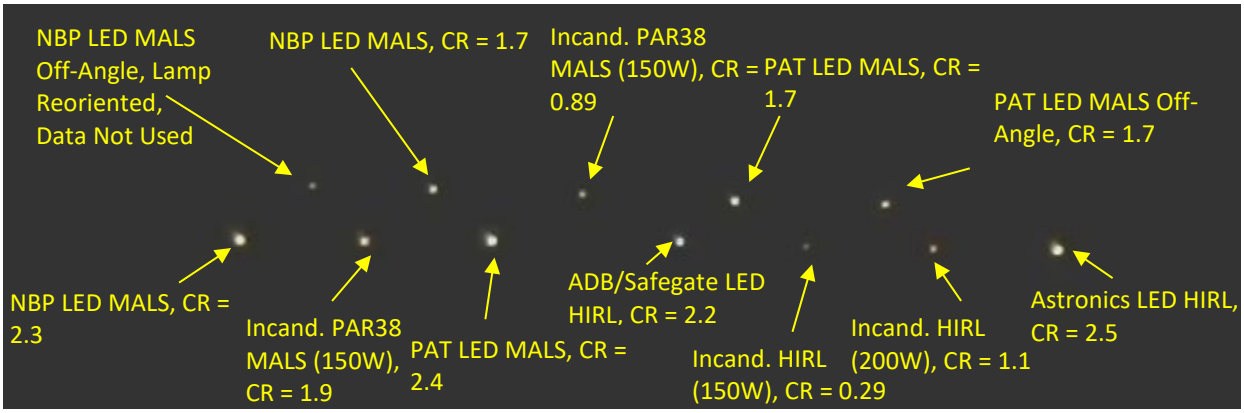

Figure A-22: January 8, 2020 at 0105 hrs

Image date and time: Jan 8, 2020 at 1:05 AM
Approximate visibility: 6,000'
METAR weather code: -SN

U.S. Department of Transportation
John A. Volpe National Transportation Systems Center
55 Broadway
Cambridge, MA 02142-1093

617-494-2000
www.volpe.dot.gov

DOT-VNTSC-FAA-21-04